Engineering Applications of Artificial Intelligence 119 (2023) 105758

Contents lists available at ScienceDirect

Engineering Applications of Artificial Intelligence

journal homepage: www.elsevier.com/locate/engappai

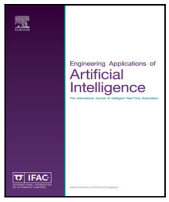

Parameter uncertainty modeling for multiobjective robust control design. Application to a temperature control system in a proton exchange membrane fuel cell

U. Veyna *, X. Blasco, J.M. Herrero, A. Pajares

Instituto de Automática e Informática Industrial - Universitat Politècnica de València, Camino de Vera S/N, Valencia, 46022, Spain

ARTICLE INFO

Keywords:
Modeling
Multiobjective optimization
Temperature control
Parameter uncertainties
Micro-CHP system
Worst-case
Robustness

ABSTRACT

Advanced control systems are tuned using dynamic models and optimization techniques. This approach frequently involves satisfying multiple conflicting objectives. Tuning robust controllers requires considering a framework that represents the system uncertainties, and its definition is not a trivial task. When dealing with a nonlinear model with many parameters, a high-quality representation requires a massive sampling of variations. In many cases, this represents an inaccessible computational cost for the optimization process.

This work presents a new methodology for parameter uncertainty modeling that is oriented to tuning robust controllers based on multiobjective optimization techniques. The uncertainty modeling formulated represents a feasible computational cost and leads to robust solutions without attributing excessive conservatism. The novelty of this process consists in using the multiobjective space to define a set of scenarios with highly representative properties of the global uncertainty framework that formulate the control problem under a predefined minimization strategy.

To demonstrate the effectiveness of this methodology, we present a temperature control design in a micro-CHP system under worst-case minimization. Based on the results, particular interest is given to verifying the appropriate formulation of the uncertainty modeling, which represents a 92.8% reduction of the computational cost involved in solving the robust optimization problem under a global uncertainty framework.

1. Introduction

Dynamic process models are currently used to adjust control systems and optimization techniques are often involved. These dynamic processes are often modeled by differential equations with parameters that are usually identified from experimental data (Godfrey, 2000). In practice, parameter models are subject to variations and uncertainties. Aerodynamic coefficients, reaction rates, inertias, masses, spring constants, and friction coefficients are common examples of these parameters in engineering processes. In an optimization control problem, even a slight modification of parameters can cause drastic effects on the solutions obtained, resulting in non-optimal performance or infeasible control (Shang et al., 2017). However, deterministic models are often used to solve control tuning problems without considering parameter uncertainties. These models become less reliable because they cannot reflect real conditions in practical applications. As a consequence, there is a need to use uncertainty models that improve the reliability of controllers and achieve performing system responses despite fluctuations (Helton, 1993). The literature shows several application examples of this approach. Robust optimization is used in Assis et al. (2018) to solve the minimization problem of the economic load dispatch of fuel required to generate electricity in a power plant. In Shang et al. (2017), the complex process of radioactive waste disposal involving significant uncertainties is assessed. In Kuo et al. (2008), a sliding mode adaptive control using the PID tuning method is proposed for trajectory tracking to control a brushless DC motor that seeks to achieve a robust system against parameter variations and external disturbances. In Kristiansson and Lennartson (2002), the design problem of robust and optimal PID controllers for a linear time invariant plant is considered based on a linear programming characterization of stabilizing PID controllers obtained by classical tuning methods. In Tan et al. (2002), a PID controller is designed to deal with performance and robust stability specifications for multivariable processes. The whole procedure is computationally simple and involves selecting several parameters. Examples show that the resulting PID settings have good time-domain performance and robustness. Fuzzy controllers are being widely used today and their applications have achieved great impact in real-world applications. In works such as Cuevas et al. (2022), Bernal et al. (2020), the optimization of a type-2 fuzzy controller for the tracking of the trajectory of an autonomous mobile robot is addressed. In this work, type-2 fuzzy controllers show a satisfactory performance

* Corresponding author.
E-mail addresses: urveyro1@doctor.upv.es (U. Veyna), xblasco@isa.upv.es (X. Blasco), juaherdu@isa.upv.es (J.M. Herrero), alpafer1@upv.es (A. Pajares).

https://doi.org/10.1016/j.engappai.2022.105758
Received 2 August 2022; Received in revised form 25 November 2022; Accepted 19 December 2022
Available online xxxx

due to their ability to handle high levels of uncertainty. In papers such as Chen et al. (2020), the heuristic tuning of a fuzzy logic controller is described to guarantee stability in a T-S fuzzy system with discrete time delay in the presence of parametric uncertainties. In Jahanshahi et al. (2020), a sliding adaptive fuzzy control design technique is proposed. The control defined is oriented to the application of four-dimensional fractional-order chaotic systems in the face of dynamic uncertainties and external disturbances.

It is possible to find works in the literature regarding different methods and techniques related to uncertainty modeling. In Gorissen et al. (2015), Assis et al. (2018), Yang et al. (2019) the use of surrogate parameter models that represent specific regions within a global uncertainty framework is encouraged. In Mckay et al. (1979), Ibrahim et al. (2019) different techniques such as pseudo random samples (PSE) or Latin hypercube samples (LHS) are described to sample variables in defined domain ranges. Defining the uncertainty framework of a system to formulate a robust optimization problem is not a simple task. In Steiner et al. (2004), Shang et al. (2017), some of the most relevant criteria to be considered in this process are discussed. It is expected that the approach explores the global framework of possible scenarios in the real system, and simultaneously represents a feasible computational cost for the optimization process. The use of methods for data model reduction and simplification is encouraged. In control problems, sensitivity analysis has been widely used to evaluate system performance under variations in the model parameter (Pianosi et al., 2016). The use of techniques for dimensional reduction (Ben-Tal and Nemirovski, 2002) such as principal component analysis (PCA) or partial least squares analysis (PLS) is also recurrent. As argued in works such as Gorissen et al. (2015), Wang and Curry (2012), the intention is to exclude uncertainty scenarios with a low probability of existing leads to the design of conservative controllers with reduced performance. A set of highly representative models of the system is required to formulate a robust control problem adequately. To take this into account, the use of different constraints that focus on the domain of uncertainties in a probabilistic region of interest must be considered in the modeling process.

In engineering processes, to represent the uncertainty framework of a system, it is often possible to describe the plant with a set of parameter models for different operating or failure conditions (Ackermann, 1985). A multi-model approach is often used to define nonlinear models as a convex combination of local models. The set of local models is combined to define a global model that is valid in the region of interest (Johansen and Murray-Smith, 1997). In papers such as Slupphaug and Foss (2000), the use of multi-models to represent partially unknown nonlinear systems is discussed. Under this concept, a control design based on LMI/BMI for a simplified Van de Vusse reactor model with parameter uncertainty is carried out. In Puschke et al. (2016), the multi-model approach to formulate a robust dynamic optimization problem using a heuristic method is addressed. With this method, the parameter models are defined according to the sensitivity of the uncertain parameters. Subsequently, this approach is applied to two case studies: a complex emulsion copolymerization process and the penicillin formation. In Gorinevsky and Stein (2003), the application of structured uncertainty modeling is presented to address robust stability analysis in a computationally efficient way. As an application, the paper formulates multidimensional models of the process, its controller, and structured uncertainty for the closed-loop control of a multidirectional paper machine process.

As previously described in most of the papers discussed above, a great effort is being made to adequately formulate control problems under the consideration of uncertainties. Since most model parameters have a real physical meaning, the importance of an appropriate representation of the uncertainties has been highlighted in the literature as an important aspect. Regarding the challenge involved in this complex task, the principal motivation for this work lies in robust control design applications. The main interest is to provide an effective method to assist the process of modeling parametric uncertainties in multivariable nonlinear systems. The aim is to define an uncertainty modeling that satisfies the essential requirements for an appropriate formulation of a control problem. These requirements are related to a low computational cost representation, the definition of highly probable scenarios, and a limitation of conservatism. Special interest is given to focus the uncertainty formulation achieved for robust controller tuning under the multiobjective optimization approach. In this paper, we propose a methodology to accomplish this task. The uncertainty representation obtained is defined by a set of models describing the different probable cases in the real application due to parameter fluctuations. The following three stages primarily describe this methodology:

In Stage 1, sensitivity analyzes are used to identify the model parameters with the most significant influence on the system performance when variations occur. This analysis derives a binary sensitivity classification of relevant and non-relevant parameters. In addition, the operating ranges in which these variations occur in the system are determined for each parameter. The justification for this stage is based on adequately defining the parameter variation ranges to avoid improbable models.

Stage 2 consists of creating a set of models focused on representing the global uncertainty framework of the system. A set of random models that entirely explores the domain of uncertainties is generated by sampling the relevant sensitivity parameters within their operating ranges. A sequence of filters is then applied to exclude models with a low probability of occurrence. This additionally reduces the computational cost of representing the uncertainty set. These filters are defined based on a deviation analysis in parameter space and an error discrepancy analysis between model and experimental system response. The exclusion of improbable models is carried out to prevent over-conservatism in the tuned controllers.

Finally, Stage 3 aims to define a representative subset of models from the set obtained in Stage 2 that improves the feasibility of the optimization approach concerning the computational cost but without reducing the quality of the uncertainty representation. For this purpose, a new strategy is used to select the most representative parameter models adequate for the uncertainty domain in a region that satisfies the robustness criterion required by the formulation of the multiobjective control problem. This sub-modeling of the uncertainty frame represents a computationally feasible cost for the optimization process.

This methodology is applied to formulate the robust temperature control problem of a proton exchange membrane fuel cell (PEMFC) stack based on multiobjective optimization. This stack is the prime mover of a micro-combined heat and power system (micro-CHP) located in our laboratory.[1] For a detailed description of the experimental equipment, see Navarro et al. (2019). A PEMFC system is a reliable and clean alternative for many power generation applications (Gimenez et al., 2020). The main advantage of these systems is the use of the thermal energy produced as a result of electricity generation that increases the overall performance of the system (Navarro et al., 2019). The electrical efficiency, lifetime of the stack, and the micro-CHP system's overall efficiency depend on correct temperature control. For proper operation, the temperature of the stack must be kept within defined limits (Zhang et al., 2013), requiring a cooling system (Wan Daud et al., 2017) to maintain its temperature at its optimum value. This cooling system must also enable the recovery of thermal energy. The durability, cost, reliability, and energy efficiency of the stack largely depend on the correct design of this cooling control system (Huang et al., 2018).

As part of a series of published papers, in Navarro et al. (2019), a nonlinear model of the cooling system of a PEMFC-based micro-CHP system is presented. This model is based on first principles, dynamic, nonlinear, and has been validated against the experimental data. The

[1] Predictive Control and Heuristic Optimization Group (CPOH), Instituto de Automática e Informática Industrial (ai2), Universitat Politècnica de València (UPV), Spain. http://cpoh.upv.es.

results show that the model can faithfully represent the dynamics of the micro-CHP cooling system. In Ferrando et al. (2020), the parametric identification of the cooling system is carried out using a multiobjective optimization approach. To develop this task, the experimental data and nonlinear model described in Navarro et al. (2019) are employed. This work highlights, as a novelty, the relevance of considering nearly optimal models nondominated in their neighborhood in problems of parametric identification. In Gimenez et al. (2020), a multiloop PID control of a PEMFC stack's temperature is designed and validated experimentally. A multiobjective optimization methodology is applied for this task, and the nonlinear model developed in Navarro et al. (2019) is used. The results obtained in these previous works provide evidence of uncertainties in several model parameters and suggest exploring a robust control approach.

As a continuation of this sequence of papers, the present work seeks to define the uncertainty modeling of the micro-CHP system oriented to the formulation of the robust control problem for the temperature control design. The PID-type control structure proposed in Gimenez et al. (2020) is implemented for this development since it is a widely used industrial control that can be easily implemented and achieves good performance. However, the uncertainty modeling methodology is independent and can be applied independently of the adopted control structure. The rest of the article is structured as follows: In Section 2, we briefly describe the problem and the properties required by uncertainty modeling to solve the robust control problem. In Section 3, we describe the proposed methodology for uncertainty modeling in nonlinear systems. In Section 4, we describe the multiobjective optimization problem formulation for the micro-CHP system's temperature control. In Section 5, we define the set of uncertainty models based on the methodology presented in this paper. In Section 6, robust control tuning is performed and the results are discussed. Finally in Section 7 we present the conclusions.

2. Uncertainty modeling approach facing the robust optimization problem

2.1. Control design problem description under multiobjective optimization approach

A classic control problem is usually aimed to control or improve the performance of a certain process during a transitory or steady state, but aspects such as minimization of control times, energy consumption, and cost reduction are not taken into account. In this situation, the optimal control design represents a very interesting alternative. Besides satisfying certain established performance conditions, it also aims for the process to achieve its best possible performance relative to a defined performance index (Ogata, 2010.). However, engineering problems continuously require situations where it is desired to optimize multiple objectives simultaneously where these objectives present some type of conflict between them (improving some objectives worsens others). This approach can be addressed using multiobjective optimization techniques. A multiobjective optimization problem (MOP) can be stated as (1)–(4) (Marler and Arora, 2004).

$$\min_{\boldsymbol{x}} \boldsymbol{f}(\mathbf{x}) = \min_{\mathbf{x}} [f_1(\mathbf{x}), f_2(\mathbf{x})] \tag{1}$$

subject to:

$$\boldsymbol{g}(\mathbf{x}) \leq 0 \tag{2}$$

$$\boldsymbol{h}(\mathbf{x}) = 0 \tag{3}$$

$$\underline{\mathbf{x}} \leq \mathbf{x} \leq \overline{\mathbf{x}} \tag{4}$$

In contrast to an optimization problem where the minimization of a single cost index is considered and a single solution is determined, the development of an MOP leads to the definition of a set of optimal solutions with different trade-offs between the design objectives, where none is better than others. This set of Pareto optimal solutions is known as the Pareto front (Huilcapi et al., 2019). The Pareto optimal set, is based on the definition of Pareto dominance (Miettinen et al., 2016) and consists of a set of solutions that are not dominated by others. In practice, optimization algorithms find a set of Pareto solutions satisfactorily. From this set, the designer can select a solution according to his preferences or design specifications.

2.2. Robust control design problem under a multiobjective optimization approach

Control tuning under a multiobjective optimization approach seeks the best system performance for multiple design objectives. Traditionally, deterministic dynamic models are used to carry out this design, assuming a level of certainty about the model parameter values. However, when the design approach intends to minimize objectives for a set of parameter uncertainties, it is possible to find sub-optimal solutions that are more interesting from a robustness perspective. As an example, Fig. 1 shows the result of an optimization problem that seeks control tuning for 2-objective minimization under consideration of a nominal parameter model $\mathbf{p}^0$ as indicated in (5). Where $\mathbf{x}$ is the parameter vector of the controller, and the functions f_1 and f_2 are the objectives to be minimized simultaneously.

$$\min_{\boldsymbol{x}} \boldsymbol{f}(\mathbf{x}, \mathbf{p}^0) = \min_{\mathbf{x}} [f_1(\mathbf{x}, \mathbf{p}^0), f_2(\mathbf{x}, \mathbf{p}^0)] \tag{5}$$

In Fig. 1, the red dots represent the Pareto front $\boldsymbol{f}(\mathbf{X}^1, \mathbf{p}^0)$ of the solution set $\mathbf{X}^1 = \{\mathbf{x}^1, \mathbf{x}^2, \ldots, \mathbf{x}^{10}\}$ obtained. The blue dot represents the sub-optimal solution $\mathbf{x}^*$ which is omitted by the optimization process. However, the relevance of this controller is highlighted when robustness under parameter uncertainties is analyzed. The upper right corner of this figure compares the degradation of the controllers $\mathbf{x}^6$ and $\mathbf{x}^*$ under the set of uncertainty models $\mathbf{A} = \{\mathbf{p}^1, \mathbf{p}^2, \ldots, \mathbf{p}^{50}\}$ generated by random parameter variations of $\mathbf{p}^0$. The light red circles represent the objective degradation $\boldsymbol{f}(\mathbf{x}^6, \mathbf{A})$ and the light blue circles represent the objective degradation $\boldsymbol{f}(\mathbf{x}^*, \mathbf{A})$. It is evident how the controller $\mathbf{x}^6$ achieves worse objective values in comparison to $\mathbf{x}^*$ for some models of set A.

Usually, finding robust solutions for nonlinear systems with many parameters requires considering a set of uncertainty models representing the different scenarios the system faces in the actual application. The definition of this framework involves adequate sampling to properly represent the system's uncertainties. On this basis, the following challenges to designing uncertainty modeling are derived:

1. Define a scanning space that thoroughly explores the domain of expected uncertainty in the system parameters.
2. Limit the inclusion of improbable models that produce over-conservative performances in the control design.
3. Define an uncertainty modeling representing a feasible computational cost for the optimization problem.

2.3. Conservatism criterion

In many situations, as shown in Fig. 1, defining more robust solutions can potentially reduce the control efficiency for system performance in the nominal case. An appropriate robustness adjustment demands a proper design of the uncertainty framework. One of the challenges of uncertainty modeling is the exclusion of improbable models that may lead to defining over-conservative controllers. To prevent the inclusion of improbable models, two criteria can be taken into account in the modeling process:

(a) The imposition of constraints on the parameter space for simultaneous variations (probabilistic criterion). As argued in works such as Gorissen et al. (2015), Shang et al. (2017), setting constraints to

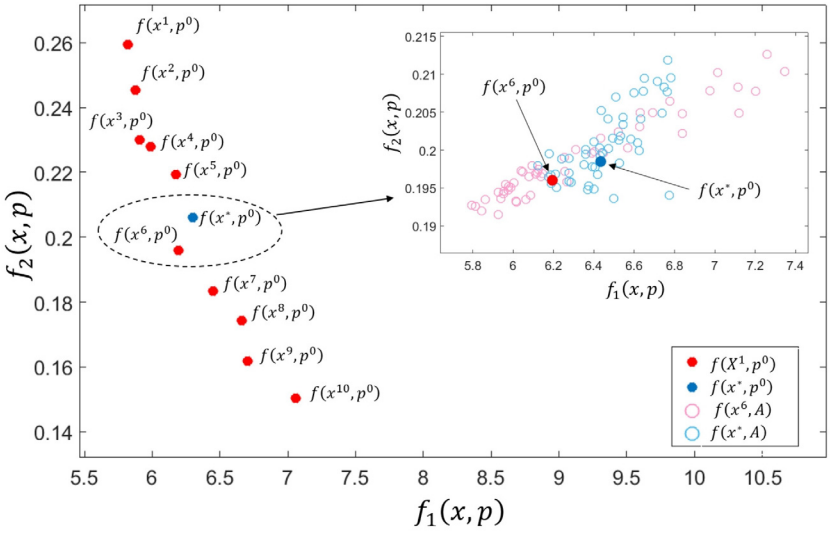

Fig. 1. Pareto front $\boldsymbol{f}(\mathbf{X}^1,\mathbf{p}^0)$ and robustness comparison between controllers $\mathbf{x}^6$ and $\mathbf{x}^*$ under parameter uncertainties.

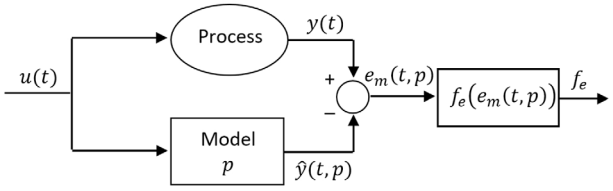

Fig. 2. Definition of function $f_e(e_m(t,\mathbf{p}))$ based on the error discrepancy between model and process responses.

define a domain D_{prob} for simultaneous deviation of uncertainties encourages discerning the more probable scenarios existing in the system. Some classical geometrical shapes used in the literature to design the domain D_{prob} where variations take place in the parameter space are the: box uncertainty set (Soyster, 1973); the Ellipsoidal uncertainty set (Ben-Tal et al., 1998); the interval + polyhedral uncertainty set; the gamma uncertainty set (Bertsimas and Sim, 2004); and the polyhedral uncertainty set (Bertsimas et al., 2010), etc.

(b) The definition of an error degradation limit $f_{e_{max}}$ (experimental criterion). As described in Spear et al. (1994), one criterion for evaluating whether a parameter model $\mathbf{p}$ is certain to exist is estimating the model error $e_m(t,\mathbf{p})$ between the model output $\hat{y}(t,\mathbf{p})$ and the system response $y(t)$ given an input signal $u(t)$ (see Fig. 2). In this sense, a tolerance restriction $f_e < f_{e_{max}}$ for defining scenarios most likely to exist is established in relation to experimental data from the validation process.

To show the application of these two criteria in the reliability validation of a model, the following example is presented: given a nonlinear 2-parameter system defined by a nominal model $\mathbf{p}^0 = [p_1^0, p_2^0]$, an uncertainty set of 50 surrogate models is defined as $\mathbf{C} = \{\mathbf{p}^1, \mathbf{p}^2, \mathbf{p}^s, \ldots, \mathbf{p}^{50}\}$. Where the model $\mathbf{p}^s = [p_1^s, p_2^s]$ represents a random parameter variation from the nominal model $\mathbf{p}^0$ within the variation ranges $\underline{p_1} \le p_1^s \le \overline{p_1}$ and $\underline{p_2} \le p_2^s \le \overline{p_2}$. Based on this example, Fig. 3 shows the different cases that can be presented when uncertainty modeling is analyzed under criteria (a) and (b). The graph on the left shows the location of the models $\{\mathbf{p}^0, \mathbf{p}^4, \mathbf{p}^{12}, \mathbf{p}^{15}, \mathbf{p}^{23}\} \in \mathbf{C}$ in the parameter space $[p_1, p_2]$. The red perimeter represents a theoretical domain D_{prob} which contains the expected simultaneous deviation of uncertainties that identifies properly probable models. Models located outside this area are classified as improbable. The right graph shows the function $f_e(e_m(t,\mathbf{p}))$ that quantifies the discrepancy based on the error between the response of a model $\mathbf{p}^s$ and the system response obtained in experimental tests (see Fig. 2). The x-axis and y-axis show the parameter space $[p_1, p_2]$. The light red plane indicates a limit defined $f_e(\mathbf{p}) = f_{e_{max}}$ to consider probable models according to the performance of each model. Models with a very high discrepancy concerning experimental data are discarded by this criterion.

The conclusion of applying this analysis to the models $\{\mathbf{p}^0, \mathbf{p}^4, \mathbf{p}^{12}, \mathbf{p}^{15}, \mathbf{p}^{23}\} \in \mathbf{C}$ is as follows:

- Nominal model $\mathbf{p}^0$ and model $\mathbf{p}^4$ satisfy both criteria.
- Model $\mathbf{p}^{12}$ satisfies criterion (a) but does not satisfy criterion (b).
- Model $\mathbf{p}^{15}$ does not satisfy either criterion (a) or criterion (b).
- Model $\mathbf{p}^{23}$ satisfies criterion (b) but does not satisfy criterion (a).

By applying these mechanisms to validate confidence in uncertainty models, it is possible to exclude improbable cases that lead to conservative controllers.

2.4. Uncertainty modeling focused on multiobjective design

In many cases, the formulation of a robust optimization problem is inaccessible due to the computational cost involved in processing the uncertainty modeling, and it becomes more complex when dealing with systems with a huge number of parameters. However, if homogeneous simplification is pursued to reduce uncertainty modeling, the quality required by the control problem approach may be excessively degraded. We propose considering the multiobjective approach in the uncertainty modeling process to define a feasible framework with valuable properties from the perspective expected by the control problem.

In works such as Cavaliere et al. (2003), Steiner et al. (2004), the Monte Carlo analysis is emphasized as the principal test to compare the robustness quality of Pareto optimal solutions. This analysis evaluates a controller under a set of uncertainty models defining control performance degradation in objective space. For modeling purposes, the principle of Monte Carlo analysis can be used to characterize surrogate models for the degradation performance they exhibit in objective space when evaluated for a set of reference controllers. To describe this approach, we present the following example: define an optimization problem that seeks control tuning for the minimization of two objectives $\boldsymbol{f} = [f_1, f_2]$ under the consideration of a nominal model $\mathbf{p}^0$, the Pareto set $\mathbf{X}^2 = \{\mathbf{x}^1, \mathbf{x}^2, \mathbf{x}^3\}$ is obtained. To represent the parameter uncertainties of the system, the set of models $\mathbf{B} = \{\mathbf{p}^1, \mathbf{p}^2, \ldots, \mathbf{p}^{10}\}$ is created. In Fig. 4 the objective degradation of each controller $\mathbf{x} \in \mathbf{X}^2$ is shown. The dotted ovals encapsulate the local degradation $\boldsymbol{f}(\mathbf{x}, \mathbf{B})$ for each controller (represented by color circles). The nominal model $\mathbf{p}^0$

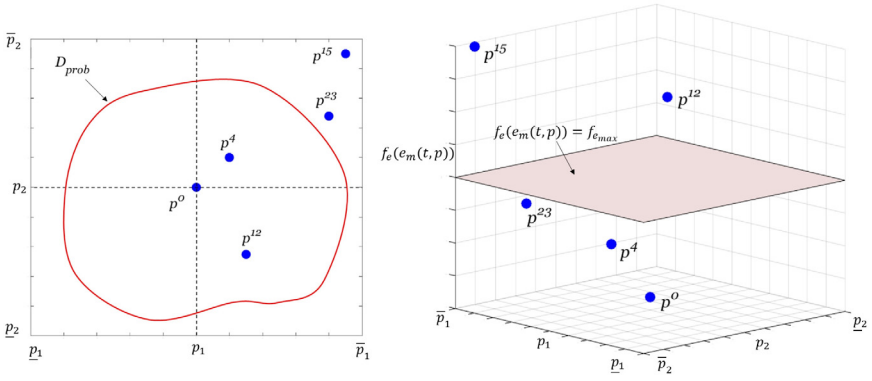

Fig. 3. Identification of reliable models. Analysis by parameter deviation is shown on the left. Analysis by discrepancy error between model and system response is shown on the right.

Table 1
Relative deviations of objective degradation in each controller $\mathbf{x} \in \mathbf{X}^2$.

Model	$\Delta f_1(\mathbf{x}^1, \mathbf{p})$	$\Delta f_2(\mathbf{x}^1, \mathbf{p})$	$\Delta f_1(\mathbf{x}^2, \mathbf{p})$	$\Delta f_2(\mathbf{x}^2, \mathbf{p})$	$\Delta f_1(\mathbf{x}^3, \mathbf{p})$	$\Delta f_2(\mathbf{x}^3, \mathbf{p})$
$\mathbf{p}^0$	0	0	0	0	0	0
$\mathbf{p}^1$	0.015	0.034	0.057	0.146	−0.028	0.016
$\mathbf{p}^2$	0.136	0.192	0.141	0.231	0.120	0.143
$\mathbf{p}^3$	−0.053	−0.056	−0.044	−0.015	−0.032	−0.056
$\mathbf{p}^4$	0.094	0.186.	0.048	0.084	0.061	0.217
$\mathbf{p}^5$	0.007	−0.051	0.015	−0.054	0.073	0.086
$\mathbf{p}^6$	0.061	0.146	0.007	0.056	0.009	0.063
$\mathbf{p}^7$	0.120	0.262	0.098	0.187	0.076	0.176
$\mathbf{p}^8$	0.035	0.064	0.039	0.033	0.036	0.033
$\mathbf{p}^9$	−0.039	0.008	−0.034	−0.089	0.017	−0.028
$\mathbf{p}^{10}$	0.093	0.113	0.094	0.121	0.049	0.139

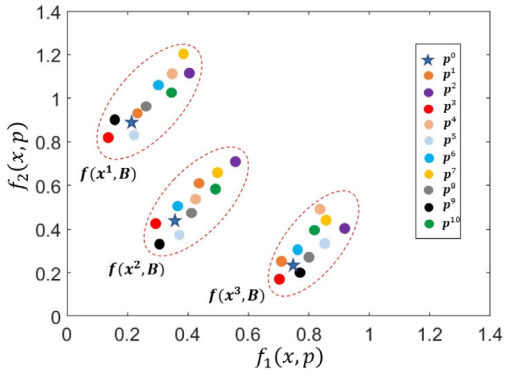

Fig. 4. Objective performance analysis for the set of optimal controllers $\mathbf{X}^2$ under $\mathbf{B}$.

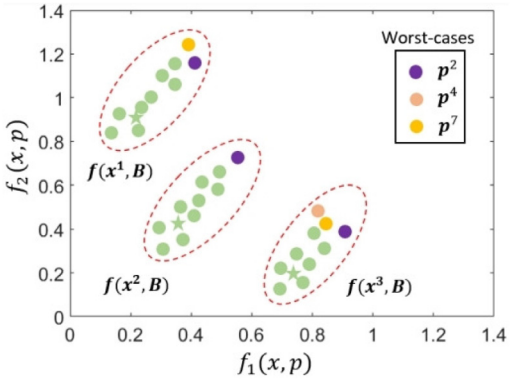

Fig. 5. Analysis for the characterization of models based on worst-case strategy.

used to determine $\mathbf{X}^2$ in the optimization problem is represented by a blue star.

Based on this analysis, we define a sub-representation of the framework $\mathbf{B}$ that contains the most relevant models that best satisfy the properties required for the optimization strategy associated with the formulation of the control problem. These models are identified with respect to their performance in the degradation analysis. The relative deviations $\Delta f_i(x, \mathbf{p}) = f_i(x, \mathbf{p}) - f_i(x, \mathbf{p}^0)$ are estimated for each uncertainty model $\mathbf{p}$ in the analysis of each controller. For the example shown in Fig. 4, the values of these deviations are presented in Table 1. To characterize uncertainty models based on their performance in the objective space, we propose alternative indices to identify models in specific regions of the degradation zone (Ide and Schöbel, 2016). Once this is achieved, the uncertainty sub-modeling is formulated and this is focused on a particular robustness strategy.

1. Worst-case uncertainty modeling

This approach aims to define a subset of models $\mathbf{B}^{wc} \subset \mathbf{B}$ for which the control system shows the worst performance concerning the design objectives. In Fig. 5, the example of this model characterization is shown.

In the objective degradation of controller $\mathbf{x}^2$, the model $\mathbf{p}^2$ is the worst-case for objectives f_1 and f_2. For both controllers $\mathbf{x}^1$ and $\mathbf{x}^3$ a worst-case front is identified by the models $\{\mathbf{p}^2, \mathbf{p}^7\}$ and $\{\mathbf{p}^2, \mathbf{p}^4, \mathbf{p}^7\}$ respectively. The set $\mathbf{B}^{wc}$ that represents the global worst-case modeling for the control system is defined from the union of the worst-case subsets defined by the analysis of each controller, therefore $\mathbf{B}^{wc} = \{\mathbf{p}^2, \mathbf{p}^4, \mathbf{p}^7\}$.

2. Goal based uncertainty modeling

This approach aims to define the subset $\mathbf{B}^{sd} \subset \mathbf{B}$ that characterizes the models with degradation quality close to a fixed position $\mathbf{d}_{\mathbf{x}^t}$ defined within the degradation zone of a controller $\mathbf{x}^t$. As an example to describe this approach, in the left graph of Fig. 6 we propose to define the set point $\mathbf{d}_{x^t} = [d_{x_1^t}, d_{x_2^t}]$ as the mean of the relative deviations for each objective, so that for the first objective $d_{x_1^t} = f_1(\mathbf{x}^t, \mathbf{p}^0) +$

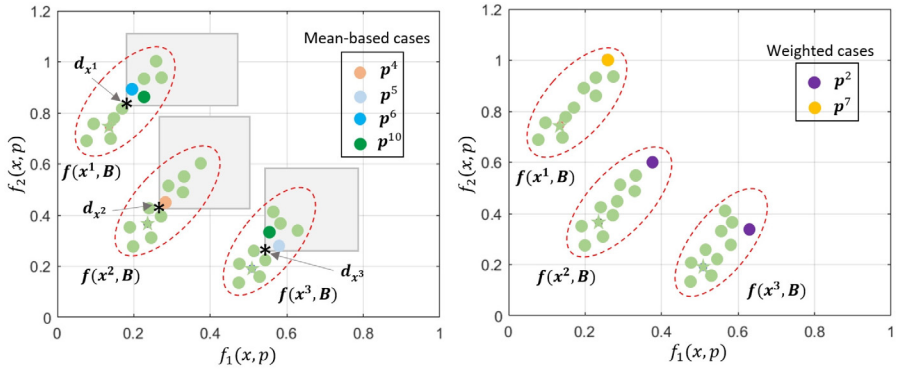

Fig. 6. Analysis for the identification of models based on goal based and weighted case strategy.

$1/10 \sum_{s=1}^{10} \Delta f_1(\mathbf{x}^t, \mathbf{p}^s)$ and for the second objective $d_{x_2^i} = f_2(\mathbf{x}^t, \mathbf{p}^0) + 1/10 \sum_{s=1}^{10} \Delta f_2(\mathbf{x}^t, \mathbf{p}^s)$.

In this figure, the black asterisk denotes the fixed points $\mathbf{d}_x^t$ and the gray rectangles represents the domain that exceeds this position. For controller $\mathbf{x^1}$, the models $\mathbf{p}^6$ and $\mathbf{p}^{10}$ minimize the approximation to point $\mathbf{d}_{x^1}$. For controller $\mathbf{x^2}$, the model $\mathbf{p}^4$ is the best approximation for both objectives. For controller $\mathbf{x^3}$, the models $\mathbf{p}^5$ and $\mathbf{p}^{10}$ are the closest to $\mathbf{d}_{x^3}$. The subset $\mathbf{B}^{sd} \subset \mathbf{B}$ representing this approach is composed of the union $\mathbf{B}^{sd} = \{\mathbf{p}^4, \mathbf{p}^5, \mathbf{p}^6, \mathbf{p}^{10}\}$.

3. Weighted case uncertainty modeling

Under this approach, the sub-modeling $\mathbf{B}^{wq} \subset \mathbf{B}$ is created from the selection of the most relevant models based on a performance-weighted ranking defined by a cost index. As an example to describe this approach, the cost index $I_c = 0.6\Delta f_1(\mathbf{x}, \mathbf{p}) + 0.4\Delta f_2(\mathbf{x}, \mathbf{p})$ is proposed to identify the worst-case scenario by giving more relevance to the degradation of objective 1 in relation to objective 2. If the measurement of the objectives have significantly different orders of magnitude, a normalization can be considered in the index's formulation. The right graph of Fig. 6 shows the representative models under this approach. The model $\mathbf{p}^7$ maximizes the index I_c for controller $\mathbf{x^1}$. For both controllers $\mathbf{x^2}$ and $\mathbf{x^3}$, the model that maximizes the index is $\mathbf{p}^2$. Note that the model selected in $\mathbf{x^1}$ predominates as the worst-case in objective 2, while the model selected in $\mathbf{x^2}$ predominates as the worst-case in objective 1. The subset $\mathbf{B}^{wq} \subset \mathbf{B}$ represents the uncertainty framework under this approach and is the union $\mathbf{B}^{wq} = \{\mathbf{p}^2, \mathbf{p}^7\}$.

3. Methodology for parameter uncertainty modeling

The methodology proposed below seeks to define an uncertainty framework to address the robust control tuning problem. Given a nonlinear system defined by a vector $\mathbf{p} = [p_1, p_2, \ldots, p_k]$ of k parameters, the definition of an uncertainty framework can be represented by a set of surrogate models $\{\mathbf{p}^s | s \in \mathbb{Z}\}$ derived from variations in $\mathbf{p}$. In this context, a surrogate model $\mathbf{p}^s$ is defined as (6).

$$\mathbf{p}^s = [p_1^s, p_2^s, p_i^s, \ldots, p_k^s] \tag{6}$$

Where p_i^s such as $1 \leq i \leq k$ denotes the variation value of parameter p_i defined in the surrogate model $\mathbf{p}^s$. These variations occur in the operating range $\underline{p_i} \leq p_i^s \leq \overline{p_i}$, where $[\underline{p_i}, \overline{p_i}]$ are the lower and upper fixed limits of sampling variations.

Initial elements. To develop this methodology, the following three elements are required:

1. Nominal model $\mathbf{p}^0$.

The model $\mathbf{p}^0$ with the nominal parameter values resulting from the identification process is expressed as:

$$\mathbf{p}^0 = [p_1^0, p_2^0, \ldots, p_k^0] \tag{7}$$

2. Error degradation limit $f_{e_{max}}$.

The error degradation limit $f_{e_{max}}$ is used to characterize probable uncertainty models concerning the error discrepancy between model and system response when evaluating a defined open-loop experiment. Its value is established based on empirical knowledge or experimental data used in the validation process when identifying nominal model $\mathbf{p}^0$. It represents a degree of tolerance for accepting surrogate models $\mathbf{p}^s$ as possible cases in the actual application. Beyond this value, degradation is quite unlikely.

3. Initial ranges of parameter variation $[\underline{pp_i}, \overline{pp_i}]$.

The ranges of variation $[\underline{pp_i}, \overline{pp_i}]$ for $i = \overline{\{1, \ldots, k\}}$ are used to initially explore the possible domain of variation in each parameter. Subsequently, these limits are fitted to the probabilistic domain of uncertainty, so their definition does not require high precision.

In Freer et al. (1996), the use of physical significance found in the existing literature is encouraged to estimate these limits. In Shang et al. (2017), it is proposed to define these limits based on a deviation from the nominal parameter values p_i^0 as indicated in (8)–(9). The constant η_i is a deviation factor defined by design criteria where variations are estimated to occur.

$$\underline{pp_i} = p_i^0 - \eta_i p_i^0 \tag{8}$$

$$\overline{pp_i} = p_i^0 + \eta_i p_i^0 \tag{9}$$

Methodology stages.

Once these three elements are defined, it is possible to develop the methodology. Fig. 7 shows a diagram with the steps, inputs, and outputs that define each stage. For better understanding, the description of each stage is detailed below.

3.1. Stage 1. Definition of operating ranges and determination of relevant and non-relevant sensitivity parameters

Objective: Estimate the operating ranges $[\underline{p_i}, \overline{p_i}]$ for $i = \{1, \ldots, k\}$ and identify the parameters of relevant and non-relevant sensitivity for the system.

Stage description: A sensitivity analysis is carried out to evaluate the individual effect of parameter variations in the model performance. Based on this analysis, the initial ranges $[\underline{pp_i}, \overline{pp_i}]$ for $i = \{1, \ldots, k\}$ are adjusted to obtain more realistic operating ranges $[\underline{p_i}, \overline{p_i}]$. The diagram in Fig. 8 describes the inputs and outputs of the steps that integrate this stage.

Step development:

- **Step 1.1: Uncertainty model definition for local sensitivity analysis.**
  As described in Pianosi et al. (2016), Helton (1993) a regional sensitivity analysis involves analyzing the performance of the system's response to variations attributed to its input factors (inputs, parameters, etc.). A wide set of guidelines for performing sensitivity analysis on a system is given in Pianosi et al. (2016). These guidelines indicate the number of models to be generated,

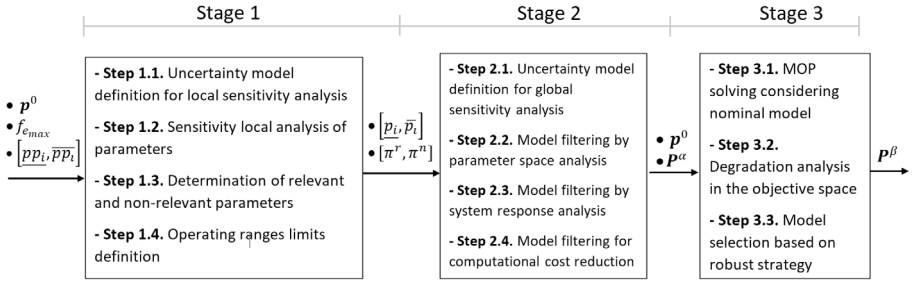

Fig. 7. General description of the steps, inputs, and outputs of the methodology for uncertainty modeling.

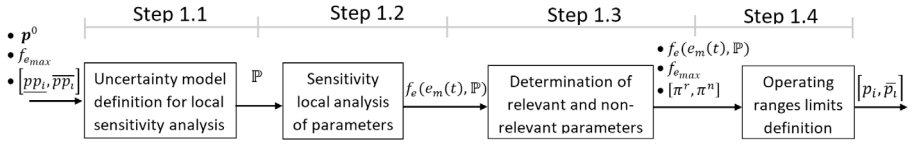

Fig. 8. Descriptive flowchart of Stage 1.

variable sampling techniques, etc. To formulate the sensitivity analysis at this stage, the set of models $\mathbb{P}$ expressed in (10) is defined.

$$\mathbb{P} = \{\mathbf{P}^i | i = \{1, \dots, k\}\} \tag{10}$$

Where $\mathbf{P}^i$ represents the set of surrogate models defined in (11)–(12), designed to analyze the individual effect of the parameter p_i. The constant h sets the number of surrogate models used to discretize the scanning range $[\underline{pp_i}, \overline{pp_i}]$, where the deviations take place.

$$\mathbf{P}^i = \{\mathbf{p}^{i,s} | s \in \mathbb{Z}, -h \leq s \leq h, s \neq 0\} \tag{11}$$

such that,

$$\mathbf{p}^{i,s} = \begin{cases} [p_1^s, p_2^0, \dots, p_k^0] & \text{if } i = 1 \\ [p_1^0, \dots, p_{i-1}^0, p_i^s, p_{i+1}^0, \dots, p_k^0] & \text{if } 1 < i < k \\ [p_1^0, \dots, p_{k-1}^0, p_k^s] & \text{if } i = k \end{cases} \tag{12}$$

If a uniform discretization of the uncertainty domain is pursued, then p_i^s can be defined as indicated in (13).

$$p_i^s = \begin{cases} p_i^0 + s\left(\frac{\overline{pp_i} - p_i^0}{h}\right) & \text{if } s > 0 \\ p_i^0 + s\left(\frac{p_i^0 - \underline{pp_i}}{h}\right) & \text{if } s < 0 \end{cases} \tag{13}$$

- **Step 1.2: Sensitivity local analysis of parameters**.
Given a model $\mathbf{p}$, the function $f_e(e_m(t, \mathbf{p}))$ evaluates the representative model quality based on the error between the model output $\hat{y}(t, \mathbf{p})$ and the measured system response $y(t)$ in an open-loop experiment (see Fig. 2). In this context, the function $f_e(e_m(t, \mathbf{P}^i))$ evaluates the performance degradation due to the deviations formulated in the set $\mathbf{P}^i$.
From the rate of change exhibited by the function $f_e(e_m(t, \mathbf{P}^i))$, the index q_i is defined. This index characterizes the sensitivity degree of the system due to the individual effect of variations in the parameter p_i. An extended review of several methods for defining the index q_i is given in Pianosi et al. (2016). Some of these are linearizations of degradation functions (Borgonovo, 2010), degradation limit approximations, multiple aggregations of individual sensitivities, and the Morris method.
If desired, a relative sensitivity ranking for the most sensitive parameter can be set by $\Delta q_i = q_i / max(\mathbf{q})$. Where $\mathbf{q} = \{q_i | i = \{1, \dots, k\}\}$.

- **Step 1.3: Determination of relevant and non-relevant parameters**.
Given the set of numerical sub-indices $\pi = \{i | i = \{1, \dots, k\}\}$ which identify the system parameters involved in (6), a binary characterization between relevant and irrelevant parameters is created by defining the subsets $\pi^r \subset \pi$ and $\pi^n \subset \pi$.
The subset π^r denotes the relevant sensitivity parameters and is defined as $\pi^r = \{i | i \in \pi, q_i > q_{min}\}$. Where q_{min} is a constant fixed by the designer and indicates the minimum value to characterize the sensitivity of a parameter as relevant or irrelevant. In contrast, the set π^n with the sub-indices of the irrelevant parameters is identified such that $\pi^n = \pi \backslash \pi^r$.
- **Step 1.4: Operating range limits definition**.
From the function $f_e(e_m(t, \mathbf{P}^i))$ and the fixed value of f_{emax}, the parameter variation limits $[\underline{p_i}, \overline{p_i}]$ are estimated as described in (14)–(15) for the relevant parameters ($i \in \pi^r$). These limits are set to avoid creating uncertainty models of implausible quality, assuming that a degradation greater than f_{emax} is unlikely.

$$\underline{p_i} = \begin{cases} p_i^s | \mathbf{p}^{i,s} \in \mathbf{P}^i, -h \leq s < 0,\ f_e(e(t, \mathbf{p}^{i,s})) \approx f_{e_{max}} & \text{if } i \in \pi^r \\ p_i^0 & \text{if } i \in \pi^n \end{cases} \tag{14}$$

$$\overline{p_i} = \begin{cases} p_i^s | \mathbf{p}^{i,s} \in \mathbf{P}^i, 0 < s \leq h,\ f_e(e(t, \mathbf{p}^{i,s})) \approx f_{e_{max}} & \text{if } i \in \pi^r \\ p_i^0 & \text{if } i \in \pi^n \end{cases} \tag{15}$$

The non-relevant sensitivity parameters are established as constants at their nominal value for the rest of the analysis since their contribution to the degradation of the system response is relatively low. Therefore $\underline{p_i} = \overline{p_i} = \mathbf{p}_i^0$ such that $i \in \pi^n$

3.2. Stage 2. Parameter uncertainty design from conservative approach

Objective: Define the set $\mathbf{P}^\alpha = \{\mathbf{p}^1, \mathbf{p}^2, \dots, \mathbf{p}^{m_\alpha}\}$ constituted by surrogate models $\mathbf{p}$ that represents the general uncertainty framework of the system under an approach that seeks to constrain conservatism.

Stage description:

The set of models $\mathbf{P}^{\phi_1}$ that explores the entire domain of uncertainties based on sampling the relevant parameters is initially defined. Subsequently, a series of filters are applied to adjust the degree of conservatism and reduce the computational cost representation. Finally, the subset of models $\mathbf{P}^\alpha \subset \mathbf{P}^{\phi_1}$ is determined as the uncertainty framework of the system. Fig. 9 shows the steps, inputs, and outputs involved in this stage.

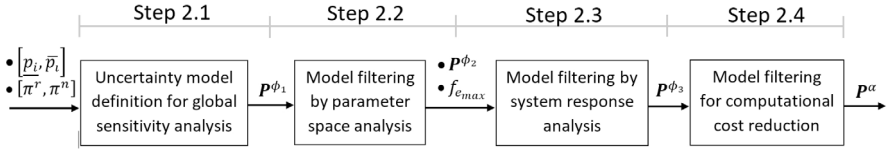

Fig. 9. Descriptive flowchart of Stage 2.

Step development:

- **Step 2.1: Uncertainty model definition for global sensitivity analysis**
  In this step, the set of models $\mathbf{P}^{\phi_1} = \{\mathbf{p}^1, \mathbf{p}^2, \dots, \mathbf{p}^{m_1}\}$ is created by simultaneous sampling of the relevant parameters ($i \in \pi^r$) such that $\underline{p_i} \leq p_i^s \leq \overline{p_i}$. Where m_1 denotes the number of models that constitute $\mathbf{P}^{\phi_1}$, and is defined by the designer on the number of parameters involved and the desired precision of the sampling (Steiner et al., 2004).
  We encourage establishing m_1 and the sampling technique according to the guidelines for global sensitivity analysis stated in Pianosi et al. (2016). These guidelines are based on the analysis of various case studies. Some of the sampling techniques mentioned here are pseudo random samples (PSE), Latin hypercube samples (LHS), and the quasi-Monte Carlo samples with Hammersley sequence sampling (HSS).
- **Step 2.2: Model filtering by parameter space analysis**
  By applying the filter defined in (16), the subset of models $\mathbf{P}^{\phi_2} \subset \mathbf{P}^{\phi_1}$ is obtained. This filter seeks to dismiss models outside of a probability domain D_{prob} (see Fig. 3).

$$\mathbf{P}^{\phi_2} = \{\mathbf{p} \in \mathbf{P}^{\phi_1} | \mathbf{p} \in D_{prob}\} \tag{16}$$

  To define the probability domain D_{prob}, a set of constraints is imposed for limiting the simultaneous deviation between parameter uncertainties in the parameter space. The designer defines these constraints based on probabilistic criteria on which it is estimated that the parameters may deviate from each other. To facilitate this task, the use of different classical constraints is encouraged (Wang and Curry, 2012; Shang et al., 2017; Gorissen et al., 2015). Some of these reported in the literature are: the box uncertainty set (Soyster, 1973); the ellipsoidal uncertainty set (Ben-Tal et al., 1998); the interval+ polyhedral uncertainty set; the gamma uncertainty set (Bertsimas and Sim, 2004); and the polyhedral uncertainty set (Bertsimas et al., 2010).
- **Step 2.3: Model filtering by system response analysis.**
  By applying the filter defined in (17), the subset $\mathbf{P}^{\phi_3} \subset \mathbf{P}^{\phi_2}$ is determined. This filter aims to exclude improbable models by analyzing the error degradation between system and model response in a defined open-loop experiment (see Fig. 2). Where the function $f_e(e_m(t, \mathbf{p}))$ is the same as the one used in step 1.2.

$$\mathbf{P}^{\phi_3} = \{\mathbf{p} \in \mathbf{P}^{\phi_2} | f_e(e_m(t, \mathbf{p})) < f_{e_{max}}\} \tag{17}$$

  The approach of using this filter to discard non-reliable models in the modeling process can be found in works such as Spear et al. (1994).
- **Step 2.4: Model filtering for computational cost reduction**.
  By using a technique for data reduction existing in the literature, we define the subset $\mathbf{P}^{\alpha} \subset \mathbf{P}^{\phi_2}$. The purpose of this latter filtering is to reduce the number of models in the set $\mathbf{P}^{\phi_3}$ (based on the designer's criteria) to obtain a suitable cost representation of uncertainties without compromising quality. The degree of reduction of this filter depends on the designer's criteria in relation to the desired computational cost. Some of the most interesting methods for data reduction are presented in Maitra and Yan (2008), such as principal component analysis (PCA) and partial least squares analysis (PLS).

At the end of this stage, the set $\mathbf{P}^{\alpha} = \{\mathbf{p}^1, \mathbf{p}^2, \dots, \mathbf{p}^{m_\alpha}\}$ that represents the system uncertainty framework under an approach that constrains conservatism and is computationally feasible is defined, where m_α is the number of models contained in $\mathbf{P}^{\alpha}$ and depends on the last modeling step of this stage.

3.3. Stage 3. Parameter uncertainty model design from multiobjective approach

Objective: Determine the subset of models $\mathbf{P}^{\beta} \subset \mathbf{P}^{\alpha}$ with the most relevant cases concerning the formulation of the multiobjective robust control problem.

Stage description:

Using the set of reference controllers $\mathbf{X}^{nom}$, we characterize the performance of the uncertainty set $\mathbf{P}^{\alpha}$ in the objective space. The set $\mathbf{X}^{nom}$ is defined by solving the multiobjective optimization problem formulated for the nominal model $\mathbf{p}^0$. Based on this analysis, the subset $\mathbf{P}^{\beta} \subset \mathbf{P}^{\alpha}$ with the most representative model is identified according to a predefined strategy that formulates the robust optimization problem. The diagram in Fig. 10 describes the inputs and outputs for the steps involved in this last stage.

Step development:

- **Step 3.1: MOP solving considering nominal model**
  To characterize the uncertainty models in the multiobjective space, it is necessary to define a set of reference controllers with good performance. In this context, the Pareto set $\mathbf{X}^{nom} = \{\mathbf{x}^1, \mathbf{x}^2, \dots, \mathbf{x}^{n_1}\}$ and its corresponding Pareto front $\mathbf{F}^{nom} = \{\boldsymbol{f}(\mathbf{x}, \mathbf{p}^0) : \mathbf{x} \in \mathbf{X}^{nom}\}$ are obtained by solving the optimization problem for the nominal model as indicated in (18).

$$\min_{\mathbf{x}} \boldsymbol{f}(\mathbf{x}, \mathbf{p}^0) \tag{18}$$

  Where n_1 is the number of solutions that constitute the Pareto set approximation.[2], $\mathbf{x}$ is the decision vector (containing the controller parameters), and $\boldsymbol{f}$ are the objectives to be minimized as defined by the designer.
- **Step 3.2: Degradation analysis in the objective space**
  Once $\mathbf{X}^{nom}$ is determined, the degradation of the Pareto front $\boldsymbol{f}(\mathbf{X}^{nom}, \mathbf{P}^{\alpha})$ is analyzed. Where the set $\boldsymbol{f}(\mathbf{x}, \mathbf{P}^{\alpha}) = \{\boldsymbol{f}(\mathbf{x}, \mathbf{p}^1), \boldsymbol{f}(\mathbf{x}, \mathbf{p}^2), \dots, \boldsymbol{f}(\mathbf{x}, \mathbf{p}^{\mathbf{m}_\alpha})\}$ describes the objective degradation of a given controller $\mathbf{x} \in \mathbf{X}^{nom}$ under the uncertainty framework $\mathbf{P}^{\alpha}$.
- **Step 3.3: Model selection based on robustness strategy.**
  Based on the degradation analysis $\boldsymbol{f}(\mathbf{x}^t, \mathbf{P}^{\alpha})$, we determine the subset $\mathbf{P}^{\beta,t} \subset \mathbf{P}^{\alpha}$ with the most relevant models in relation to its performance in the objective space concerning controller $\mathbf{x}^t$.
  The subset of models $\mathbf{P}^{\beta,t}$ is defined in the degradation analysis for each controller $\mathbf{x}^t \in \mathbf{X}^{nom}$ such that $t = \{1, \dots, n_1\}$ according to one of the proposed strategies shown in Section 2.3 for model selection.
  The set of models $\mathbf{P}^{\beta} = \{\mathbf{p}^1, \mathbf{p}^2, \dots, \mathbf{p}^{m_\beta}\}$ is made from the union of the subsets $\mathbf{P}^{\beta,t}$ as indicated in (19). This set represents the most relevant models concerning degradation analysis $\boldsymbol{f}(\mathbf{X}^{nom}, \mathbf{P}^{\alpha})$ with the most relevant models $\mathbf{p} \in \mathbf{P}^{\alpha}$ for the formulation of the robust

[2] Multiobjective optimization algorithms obtain an approximation to the Pareto set.

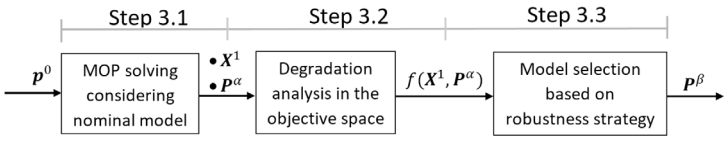

Fig. 10. Descriptive flowchart of Stage 3.

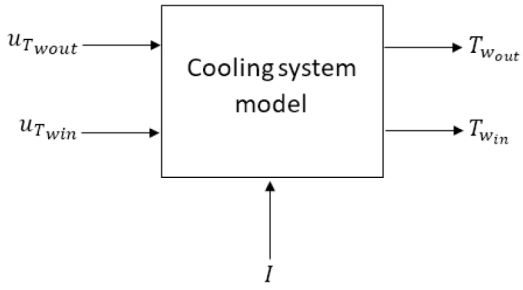

Fig. 11. Black box diagram of the model.

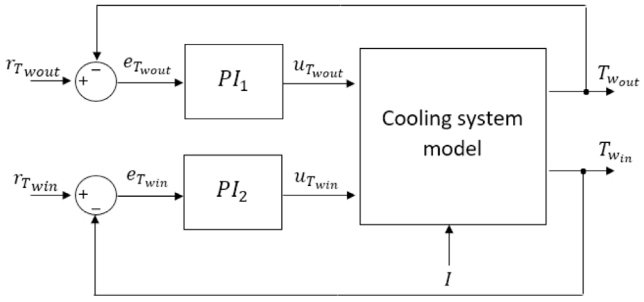

Fig. 12. Multiloop PI control structure for temperatures T_{wout} and T_{win}.

optimization problem under a predefined minimization strategy. Where m_β is the total number of models that constitutes $\mathbf{P}^\beta$ and is defined by the characterization process.

$$\mathbf{P}^\beta = \mathbf{P}^{\beta,1} \cup \mathbf{P}^{\beta,2} \cup, \ldots, \mathbf{P}^{\beta,n_1} \tag{19}$$

4. Multiobjetive control problem formulation under parameter uncertainties

4.1. PEMFC model description

The PEMFC stack that is located in our laboratory, is supplied with hydrogen and air to generate electrical energy and heat. A programmable electronic load is used to emulate a residential consumption of electricity (electrical appliances). A radiator simulates the heat energy consumption (hot water and heating) by extracting heat when activated. Additionally, thermal energy can be stored in a water tank.

For the PEMFC stack temperature control design, a model of the cooling circuit of the micro-CHP system was used. Fig. 11 shows a black box diagram of the model detailed in Gimenez et al. (2020). The model has two outputs related to the liquid coolant: the stack water outlet and inlet temperatures $T_{w_{out}}$ and $T_{w_{in}}$. The control actions are $u_{T_{wout}}$, which represents the water flow rate in the primary cooling circuit, and $u_{T_{win}}$, which is the water flow rate in the secondary cooling circuit (for more details see Gimenez et al. (2020)). The only disturbance considered is the electric current (I) demanded by the stack. This nonlinear dynamic model is built from first principles and was experimentally validated with a wide operating range (from 140 to 200A).

The model has 30 parameters that represent the physical magnitudes of the plant. This nonlinear dynamic model is used for the design of temperature control. In Navarro et al. (2019), details of the parameter identification and validation of a nominal model for the cooling system can be found. In Ferrando et al. (2020), near-optimal models are analyzed, and an approximation of the operating ranges for the parameter uncertainties when the system operates around its set-point is presented.

4.2. Temperature control structure

The aim of the control system is to keep $T_{w_{out}}$ and $T_{w_{in}}$ at their corresponding setpoints while changes in the electrical current demand (I) produce undesirable transient fluctuations in the stack temperature, resulting in a loss of electrical efficiency or in an increased deterioration of the stack. The temperature control must respond disturbances to minimize the excursions of $T_{w_{out}}$ and $T_{w_{in}}$ from their setpoints, $r_{T_{wout}} = 65°C$ and $r_{T_{wout}} = 60°C$, respectively. Gimenez et al. (2020) proposes a multiloop control structure (see Fig. 12), this structure consists of two PI controllers with anti-windup, one for the control of $T_{w_{out}}$ (by using $u_{T_{wout}}$) and the other for the control of $T_{w_{in}}$ (by using $u_{T_{win}}$). Therefore, the controller has four parameters to adjust (two for each PI), $\mathbf{x} = [K_{c1}, T_{i1}, K_{c2}, T_{i2}]$, where K_{c1} and K_{c2} are in ((l/min)/°C) and T_{i1} and T_{i2} in (s).

4.3. Formulation of the multiobjective control problem under uncertainties

The multiobjective problem of temperature control tuning under parameter uncertainties aims to minimize the objectives f_1 and f_2 as formulated in Eqs. (20) and (21).

$$f_1(\mathbf{x}, \mathbf{p}) = \frac{1}{T_{sim}} \int_0^{T_{sim}} |e_{T_{w_{out}}}| dt + \frac{1}{T_{sim}} \int_0^{T_{sim}} |e_{T_{w_{in}}}| dt \tag{20}$$

$$f_2(\mathbf{x}, \mathbf{p}) = \frac{1}{T_{sim}} \int_0^{T_{sim}} \left| \frac{du_{T_{w_{out}}}(t)}{dt} \right| dt + \frac{1}{T_{sim}} \int_0^{T_{sim}} \left| \frac{du_{T_{w_{in}}}(t)}{dt} \right| dt \tag{21}$$

Where $\mathbf{p}$ is the vector of model parameters defined in (22) and $\mathbf{x}$ is the decision vector (containing the controller parameters). $\underline{\mathbf{x}}$ and $\overline{\mathbf{x}}$ are the lower and upper bounds for controller tuning (Eq. (24)).

$$\mathbf{p} = [p_1, p_2, \ldots, p_k] \tag{22}$$

$$\mathbf{x} = [K_{c1}, T_{i1}, K_{c2}, T_{i2}] \tag{23}$$

$$\underline{\mathbf{x}} = [\underline{K_{c1}}, \underline{T_{i1}}, \underline{K_{c2}}, \underline{T_{i2}}]; \ \overline{\mathbf{x}} = [\overline{K_{c1}}, \overline{T_{i1}}, \overline{K_{c2}}, \overline{T_{i2}}] \tag{24}$$

Objective $f_1(\mathbf{x}, \mathbf{p})$ evaluates the performance of the controllers by adding the mean absolute errors of the stack output and input temperatures (in °C) concerning their setpoints (Eqs. (25) and (26)).

$$e_{T_{w_{out}}} = r_{T_{w_{out}}} - T_{w_{out}} \tag{25}$$

$$e_{T_{w_{in}}} = r_{T_{w_{in}}} - T_{w_{in}} \tag{26}$$

Objective $f_2(\mathbf{x}, \mathbf{p})$ evaluates the control effort by adding the average absolute values of the rates of change of the control actions ($u_{T_{w_{out}}}$ and $u_{T_{w_{in}}}$) in $(l/min)/s$. T_{sim} is the simulation time (3300s). The aim of the objectives f_1 and f_2 is to achieve an optimal electrical efficiency and a minimal deterioration of the stack and actuators.

The temperature control should respond to changes in the electric current demand. Fig. 13 shows the electric current signal used for the

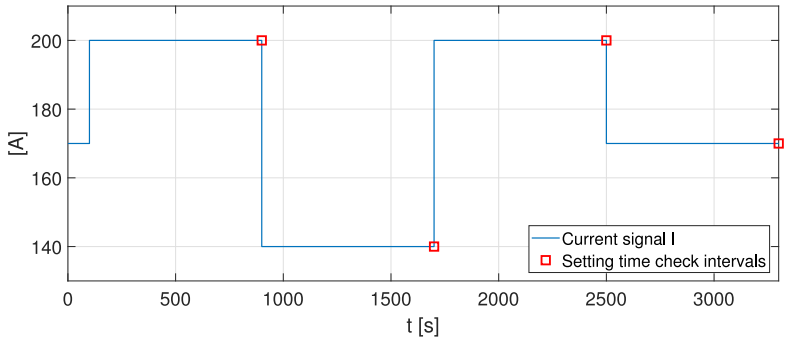

Fig. 13. Electric current demand signal used in the control design. The first step applied is at $t = 100$ s, and the span of each step is 800 s. The total simulation time is 3300 s.

control design that presents steps and traverses through the full validity range of the nonlinear model (from 140 to 200A).

Given these conditions, the multiobjective optimization problem is formulated as follows:

$$\min_{\mathbf{x}} \boldsymbol{f}(\mathbf{x}, \mathbf{p}^0) \tag{27}$$

$$\boldsymbol{f}(\mathbf{x}, \mathbf{p}^0) = [f_1(\mathbf{x}, \mathbf{p}^0), f_2(\mathbf{x}, \mathbf{p}^0)] \tag{28}$$

subjet to:

$$\underline{\mathbf{x}} \leq \mathbf{x} \leq \overline{\mathbf{x}} \tag{29}$$

$$\underline{\mathbf{x}} = [-8, 1, -8, 1] \tag{30}$$

$$\overline{\mathbf{x}} = [-0.1, 120, -0.1, 120] \tag{31}$$

$$|e_{T_{w_{out}}}(n)| < 0.033\ ^\circ\text{C} \tag{32}$$

$$|e_{T_{w_{in}}}(n)| < 0.033\ ^\circ\text{C} \tag{33}$$

The optimization problem must satisfy some additional settling time constraints, which are formulated as shown in (32) and (33), where n are the sampling times corresponding to 1 s before each change in the disturbance signal. In Fig. 13, the location of the time intervals at which these steady-state conditions are verified is marked with red squares.

For robust controller tuning, an uncertainty framework must be considered. As proposed in the methodology, the most relevant uncertainty models to address this formulation will be collected by the set $\mathbf{P}^\beta = \{\mathbf{p}^1, \mathbf{p}^2, \ldots, \mathbf{p}^{m_\beta}\}$. The multiobjective problem must then be reformulated for robustness:

$$\min_{\mathbf{x}} \boldsymbol{f}_{max}(\mathbf{x}, \mathbf{P}^\beta) \tag{34}$$

$$\boldsymbol{f}_{max}(\mathbf{x}, \mathbf{P}^\beta) = [f_{1_{max}}(\mathbf{x}, \mathbf{P}^\beta), f_{2_{max}}(\mathbf{x}, \mathbf{P}^\beta)] \tag{35}$$

Where $f_{1_{max}}(\mathbf{x}, \mathbf{P}^\beta)$ and $f_{2_{max}}(\mathbf{x}, \mathbf{P}^\beta)$ define the robustness strategy. For this particular case, we propose to pursue a minimization concerning the worst-case index, so that:

$$f_{1_{max}}(\mathbf{x}, \mathbf{P}^\beta) = \max_{\forall p \in \mathbf{P}^\beta} (f_1(\mathbf{x}, \mathbf{p})) \tag{36}$$

$$f_{2_{max}}(\mathbf{x}, \mathbf{P}^\beta) = \max_{\forall p \in \mathbf{P}^\beta} (f_2(\mathbf{x}, \mathbf{p})) \tag{37}$$

This optimization problem is also subjected to constraints (29)–(33).

5. Definition of the uncertainty modeling of the PEMFC system

As described in the formulation of the robust control problem, it is necessary to define the uncertainty set of models $\mathbf{P}^\beta$ for tuning control gains. This section shows the development of the methodology presented in Section 3 applied to the PEMFC system. The three input elements required are defined as follows:

5.1. Initial elements

1. **The nominal parameter model**
   From the identification and validation process (Navarro et al., 2019), the nominal model is defined by $k = 31$ parameters that constitute the vector $\mathbf{p}^0 = [p_1^0, p_2^0, \ldots, p_{31}^0]$. These values are presented in Table 2. As consideration for this analysis, the parameters $cal_{T_{a_{out}}}$, $cal_{T_{pH_{out}}}$, $cal_{T_{w_{out}}}$ are considered fixed since they belong to calibration constants and the parameter $pemfc_{eff}$ that characterizes the battery efficiency is added.
2. **Degradation limit for system response**
   From the experiment performed in the validation process, an average temperature error $f_e(e_m(t, \mathbf{p}^0)) = 0.26\ ^\circ$C is associated with the identified nominal model (see the model validation test in Navarro et al. (2019)). On the basis of this data, the degradation limit $f_{e_{max}} = 0.5\ ^\circ$C is established as a degree of tolerance for the classification of uncertainty models with acceptable reliability.
3. **Initial ranges of variation for each parameter**
   To define the scanning ranges $[\underline{pp_i}, \overline{pp_i}]$ on which the domain of uncertainty is initially explored, we propose to use a range defined by the deviation of ±95% of the nominal value of each parameter. Using this range, we seek to ensure a full exploration of the variations that enables determining the sensitivity and appropriate operating ranges of each parameter. Therefore $\underline{pp_i} = p_i^0 - 0.95p_i^0$ and $\overline{pp_i} = p_i^0 + 0.95p_i^0$ for $i = \{1, \ldots, k\}$. For the particular case of parameter p_{31} (battery efficiency degradation) only variation in negative direction is considered, and therefore $\overline{pp}_{31} = 0$ is fixed.

Once these three input elements are defined, each stage of the methodology is developed as follows.

5.2. Description of stage 1

- *Step 1.1*
  Based on the guidelines established in Pianosi et al. (2016) for performing local analysis, we set $h = 19$ as the number of surrogate models used to uniformly discretize the range $[\underline{pp_i}, \overline{pp_i}]$ and carry out the sensitivity analysis for each parameter. Therefore, $\mathbf{P}^i$ for $i = \{1, \ldots, k\}$ is defined as indicated in (38).

$$\mathbf{P}^i = \{\mathbf{p}^{i,s} | s \in \mathbb{Z}, -19 \leq s \leq 19, s \neq 0\} \tag{38}$$

such that,

$$\mathbf{p}^{i,s} = \begin{cases} [p_1^s, p_2^0, \ldots, p_{31}^0] & \text{if } i = 1 \\ [p_1^0, \ldots, p_{i-1}^0, p_i^s, p_{i+1}^0, \ldots, p_{31}^0] & \text{if } 1 < i < 31 \\ [p_1^0, \ldots, p_{k-1}^0, p_{31}^s] & \text{if } i = 31 \end{cases} \tag{39}$$

and,

$$p_i^s = \begin{cases} p_i^0 + s\left(\frac{\overline{pp_i} - p_i^0}{19}\right) & \text{if } s > 0 \\ p_i^0 + s\left(\frac{p_i^0 - \underline{pp_i}}{19}\right) & \text{if } s < 0 \end{cases} \tag{40}$$

Table 2
Summary of nominal values p_i^s, operating range limits $[\underline{p_i}, \overline{p_i}]$ and relative sensitivity indices Δq_i for each parameter p_i.

Parameter tag	p_i	p_i^0	$\underline{p_i}$	$\overline{p_i}$	Δq_i	π^r/π^n
$cal_{Ta_{out}}$	p_1	0.81	0.04	1.57	2e−4	Non-sensitive
$cal_{Tp4_{out}}$	p_2	0.25	0.01	0.48	2e−4	Non-sensitive
$cal_{Tw_{out}}$	p_3	1.01	0.05	1.96	2e−4	Non-sensitive
$h_{a_{max}}$	p_4	52.01	16.06	101.42	0.023	Sensitive
$h_{a_{min}}$	p_5	26.13	5.94	50.95	0.015	Non-sensitive
h_{atw}	p_6	40.89	20.03	79.73	0.023	Sensitive
$h_{fc_{loss}}$	p_7	3.39	1.67	5.39	0.023	Sensitive
$h_{fc_{2max}}$	p_8	44.78	2.23	87.32	6e−3	Non-sensitive
$h_{fc_{2min}}$	p_9	15.71	0.78	30.63	3e−4	Non-sensitive
$h_{p1_{loss}}$	p_{10}	8.11	6.46	9.73	0.06	Sensitive
$h_{p4_{loss}}$	p_{11}	8.28	6.11	10.40	0.046	Sensitive
$h_{rOFF_{max}}$	p_{12}	9.74	0.48	18.99	0.006	Non-sensitive
$h_{rOFF_{min}}$	p_{13}	8.17	2.35	15.03	0.016	Non-sensitive
$h_{rON_{max}}$	p_{14}	1.02e2	91.21	110.35	0.164	Sensitive
$h_{rON_{min}}$	p_{15}	59.33	52.24	64.71	0.132	Sensitive
$h_{s_{max}}$	p_{16}	2.31e2	66.79	451.01	0.021	Sensitive
$h_{s_{min}}$	p_{17}	54.07	10.82	105.45	0.022	Sensitive
ht_{max}	p_{18}	83.91	43.55	163.64	0.024	Sensitive
$h_{t_{min}}$	p_{19}	22.02	1.10	42.93	0.28e−2	Non-sensitive
$h_{w_{max}}$	p_{20}	66.37	16.75	129.42	0.020	Sensitive
$h_{w_{min}}$	p_{21}	57.48	2.87	112.09	0.46e−2	Non-sensitive
k_a	p_{22}	52.65e2	37.65e2	66.78e2	0.044	Sensitive
T_{amb_r}	p_{23}	27.17	26.06	28.09	0.356	Sensitive
V_a	p_{24}	28.21e−4	27.87e−4	55.01e−4	1.00	Sensitive
V_{p1}	p_{25}	4.8e−4	2.4e−5	93.6e−5	2e−4	Non-sensitive
V_{p4}	p_{26}	15.7e−4	7.85e−5	30.61e−4	6e−4	Non-sensitive
V_r	p_{27}	10.4e−4	5.2e−5	20.28e−4	13e−4	Non-sensitive
V_{t1}	p_{28}	19.4e−4	9.7e−5	37.83e−4	21e−4	Non-sensitive
V_{t2}	p_{29}	28.67e−3	12.11e−3	55.91e−3	0.021	Sensitive
V_w	p_{30}	12.5e−4	6.25e−5	24.37e−4	0.001	Non-sensitive
$pemfc_{eff}$	p_{31}	99.32e−2	96.05e−2	1.93	0.363	Sensitive

- *Step 1.2*

Based on the system model and the same open-loop experiment used in the parameter validation process, the function $f_e(e_m(t,\mathbf{p}))$ is computed to evaluate the sets of models $\mathbf{P}^i \in \mathbb{P}$. In this test (see Fig. 2), both the model and the system are excited with the same input signals (see Figure 5 of Navarro et al. (2019) to view the input signals) for a simulation time of $T_{sim} = 8087s$. As introduced in Navarro et al. (2019), the output of the complete model consists of the 6 temperatures $T_{w_{out}}, T_{w_{in}}, T_{t2}, T_{a_{out}}, T_{s_{in}}$ and $T_{s_{out}}$. Therefore, the average absolute error of the system output is determined as indicated in (41), which represents the aggregated error function for the comparison between the six model outputs with the six real system outputs (42)–(47). The variables with a cap denote the process outputs and the variables without cap denote the model outputs.

$$f_e(e_m(t,\mathbf{p})) = (J_1 + J_2 + J_3 + J_4 + J_5 + J_6)/6 \tag{41}$$

$$J_1 = \frac{1}{T_{sim}} \int_0^{T_{sim}} |\hat{T}_{w_{out}}(t) - T_{w_{out}}(t)|dt \tag{42}$$

$$J_2 = \frac{1}{T_{sim}} \int_0^{T_{sim}} |\hat{T}_{w_{in}}(t) - T_{w_{in}}(t)|dt \tag{43}$$

$$J_3 = \frac{1}{T_{sim}} \int_0^{T_{sim}} |\hat{T}_{t2}(t) - T_{t2}(t)|dt \tag{44}$$

$$J_4 = \frac{1}{T_{sim}} \int_0^{T_{sim}} |\hat{T}_{a_{out}}(t) - T_{a_{out}}(t)|dt \tag{45}$$

$$J_5 = \frac{1}{T_{sim}} \int_0^{T_{sim}} |\hat{T}_{s_{in}}(t) - T_{s_{in}}(t)|dt \tag{46}$$

$$J_6 = \frac{1}{T_{sim}} \int_0^{T_{sim}} |\hat{T}_{s_{out}}(t) - T_{s_{out}}(t)|dt \tag{47}$$

The function $f_e(e_m(t,\mathbf{P^i}))$ defines the error degradation due to the parameter deviations formulated in set $\mathbf{P^i}$ to analyze the parameter p_i. As an example to illustrate this analysis, Fig. 14 exhibits the functions $f_e(e_m(t,\mathbf{P^{22}}))$ and $f_e(e_m(t,\mathbf{P^{18}}))$. The performance of these functions exhibits the sensitivity of the system output error due to incremental deviations over the parameters p_{22} and p_{18}. Where the x-axis indicates the models $\mathbf{p}^{i,s} \in \mathbf{P}^i$ such that $-h \le s \le h$ and y-axis shows the average absolute error $f_e(e_m(t,\mathbf{p}))$ in [°C]. The red dotted line indicates the degradation limit stated in $f_{e_{max}} = 0.5$ °C. From the performance shown in Fig. 14, it is possible to realize that variations on p_{22}^s produce a higher rate of change in the output error with respect to variations on p_{18}^s since the function $f_e(e_m(t,\mathbf{P}^{22}))$ overshoots the limit $f_{e_{max}}$ for a model with lower relative deviation than $f_e(e_m(t,\mathbf{P}^{18}))$. This same analysis is carried out to analyze the rate of change in each error degradation function defined for the remaining sets $\mathbf{P}^i \in \mathbb{P}$.

To characterize the degree of sensitivity, the coefficient $q_i = max(|\underline{q_i}|, |\overline{q_i}|)$ is determined for each parameter. Where $\underline{q_i}$ and $\overline{q_i}$ are defined as indicated in (48)–(49).

$$\underline{q_i} = \left\{ \frac{\Delta f_e}{s} | -h \le s < 0;\ f_e(e_m(t,\mathbf{p}^{i,s})) \approx f_{e_{max}} \right\} \tag{48}$$

$$\overline{q_i} = \left\{ \frac{\Delta f_e}{s} | 0 < s \le h;\ f_e(e_m(t,\mathbf{p}^{i,s})) \approx f_{e_{max}} \right\} \tag{49}$$

The ratio $\Delta f_e/s$ represents a slope, where $\Delta f_e = f_e(e_m(t,\mathbf{p}^{i,s})) - f_e(e_m(t,\mathbf{p}^0))$ such that $f_e(e_m(t,\mathbf{p}^{i,s})) \approx f_{e_{max}}$. Given the set $\mathbf{q} = \{q_i | i = \{1,\dots,k\}\}$, which contains the sensitivity coefficients of all the parameters, we define the normalized coefficients $\Delta q_i = q_i/max(\mathbf{q})$ concerning the coefficient of the parameter with the highest degree of sensitivity. The values of coefficients Δq_i are shown in Table 2.

- *Step 1.3*

Based on a design criterion, non-relevant sensitivity parameters are considered due to the fact that its sensitivity coefficients are $\Delta q_i < 0.02$, which represents a significantly lower sensitivity in relation to the most sensitive parameter. This condition is established based on the observation that 15 parameters represent a relative sensitivity of less than 2% concerning the most

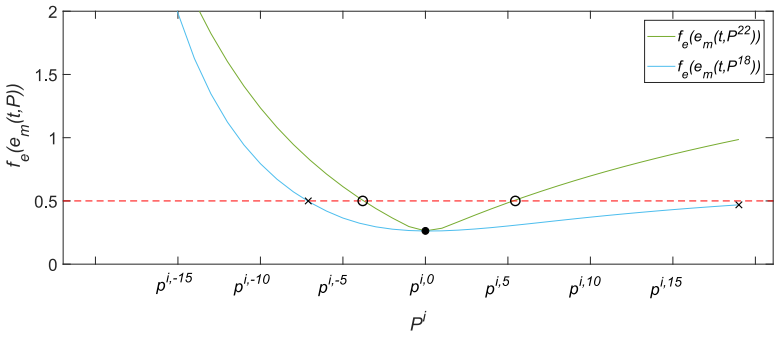

Fig. 14. Analysis of the temperature error degradation due to the effect of variations on p^s_{18} and p^s_{22}.

sensitive parameter; this enables the uncertainty modeling to focus on variations in the most sensitive parameters and reduce computational cost. Therefore, the sets π^r and π^n are defined as follows: $\pi^r = \{4, 6, 10, 11, 14, 15, 16, 17, 18, 20, 22, 23, 24, 29, 31\}$ and $\pi^n = \{1, 2, 3, 5, 7, 8, 9, 12, 13, 19, 21, 25, 26, 27, 28, 30\}$.

- *Step 1.4*
  From the analysis shown in Fig. 14, the operating range limits $[\underline{p_i}, \overline{p_i}]$ are estimated for the relevant sensitivity parameters ($i \in \pi_r$) by using Eqs. (15)–(14). These equations identify the deviation p^s_i that best approximates the limit $f_e(e_m(t, \mathbf{P}^i)) \approx f_{e_{max}}$. In Fig. 14, the limits $[\underline{p_i}, \overline{p_i}]$ for p^s_{22} and p^s_{18} are marked with crosses and circles respectively. The range of variation for the negligent sensitivity parameters ($i \in \pi_n$) are restricted to the nominal value, this is $\underline{p_i} = \overline{p_i} = p^0_i$.
  Finally, Table 2 shows the conclusion of the analysis performed at this stage. Where the upper and lower operating range limits $[\underline{p_i}, \overline{p_i}]$ and the relative sensitivity index Δq_i of the k parameters considered at the beginning of the analysis are shown.

5.3. Description of stage 2

- *Step 2.1*
  The set $\mathbf{P}^{\phi_1} = \{\mathbf{p}^1, \mathbf{p}^2, \ldots, \mathbf{p}^{m_1}\}$ is created from the random sampling of deviations $p^s_i \in \mathbf{p}^s$ such that $\underline{p_i} \leq p^s_i \leq \overline{p_i}$. The amount of models $m_1 = 1500$ is established based on the number of parameters for which uncertainties are considered (100 models per each relevant sensitivity parameter) according to the guidelines stated for performing a sensitivity analysis for global mapping (these guidelines are summarized in Figure 3 in Pianosi et al. (2016)).
- *Step 2.2*
  The model filter indicated in (16) is applied to obtain the subset $\mathbf{P}^{\phi_2} \subset \mathbf{P}^{\phi_1}$ with probable models that belong to the domain D_{prob} (see Fig. 3). To design the domain D_{prob}, we use the classical ellipsoidal uncertainty set (Ben-Tal et al., 1998) chosen for geometrically fitting the domain of the system parameter variations. By using this concept, we define the model filter indicated in (50).

$$\mathbf{P}^{\phi_2} = \{\mathbf{p} \in \mathbf{P}^{\phi_1} \,|\, \tau_{wy} < r_{max}, \forall y, w, w \neq y\} \tag{50}$$

Where the coefficient τ_{wy} indicated in (51) characterizes the simultaneous parameter deviation of the uncertainties p^s_w and p^s_y in model $\mathbf{p}^s$, for all $1 \leq y, w \leq k$ such that $w \neq y$.

$$\tau^s_{wy} = \sqrt{(\delta^s_w)^2 + (\delta^s_y)^2} \tag{51}$$

The coefficient δ^s_i is defined in (52) and represents the relative parameter deviation of p^s_i with respect to its operating range $[\underline{p_i}, \overline{p_i}]$ such that $0 \leq \delta^s_i \leq 1$.

$$\delta^s_i = \begin{cases} (p^s_i - p^0_i)/(\overline{p_i} - p^0_i) & \text{if} \quad p^s_i - p^0_i > 0 \\ (p^0_i - p^s_i)/(p^0_i - \underline{p_i}) & \text{if} \quad p^s_i - p^0_i < 0 \\ 0 & \text{if} \quad p^s_i - p^0_i = 0 \end{cases} \tag{52}$$

To apply (50), we establish a limit of $r_{max} = 0.85\sqrt{2}$, which defines a relative deviation of 85% between any two parameters simultaneously in a model uncertainty. A similar formulation can be followed in Wang and Curry (2012).

- *Step 2.3*
  In this step, the subset of models $\mathbf{P}^{\phi_3} \subset \mathbf{P}^{\phi_2}$ is defined based on the filter indicated in Eq. (17), which categorizes the probable models based on the condition $f_e(e_m(t, \mathbf{p})) < 0.5$.
- *Step 2.4*
  A last model reduction is applied to obtain the subset $\mathbf{P}^{\alpha} \subset \mathbf{P}^{\phi_3}$, which is defined as a representative sample of the uncertainty framework $\mathbf{P}^{\phi_3}$ with a suitable computational cost. We choose to use the PCA method, which enables us to obtain uniformly distributed models in the range of the mapped variance and identify regions in the sampling space where the model prediction is representative of the global set (for details of its application, see Kamali et al. (2007)). For this purpose, we reduced the size of the set $\mathbf{P}^{\phi_3}$ to 140 models, since it represents approximately one fourth of $dim(\mathbf{P}^{\phi_3})$.

Finally, Fig. 15 shows the conclusion of the model reduction process at this stage. Where the Y-axis denotes the evaluation of the function $f_e(e(t, \mathbf{p}))$ and the x-axis indicates the global relative deviation $\gamma(\mathbf{p})$ defined in (53).

$$\gamma^s = \sqrt{\sum_{i=1}^{k} (\delta^s_i)^2} \tag{53}$$

At first, the uncertainty modeling process begins with the set $\mathbf{P}^{\phi_1}$, which is defined with 1500 models generated by random sampling within the operating range established in the sensitivity analysis. In Fig. 15 this set of models is represented for all the green, black and red dots. By applying the first filter (step 2.2), improbable models concerning the parameter space analysis are excluded. Therefore, the set $\mathbf{P}^{\phi_2}$ of 1071 models (black and red dots) is defined. By applying the second filter (step 2.3) based on the analysis of the model's performance and the constraint $f_e(e_m(t, \mathbf{p})) < 0.5$ °C, the set $\mathbf{P}^{\phi_3}$ of 573 models (red dots) is obtained.

Finally, the last filter is used to uniformly simplify the modeling to a computationally acceptable representation for the next stage. We consider 140 models (approximately 25% of the size set $\mathbf{P}^{\phi_3}$) as a good size of representation to create the set $\mathbf{P}^{\alpha}$ (blue circles).

5.4. Description of stage 3

- *Step 3.1*
  The optimization problem described by the Eqs. (20)–(33) is solved for the nominal model. As result, the Pareto set $\mathbf{X}^{nom} = (\mathbf{x}^1, \mathbf{x}^2, \ldots, \mathbf{x}^{11})$ is obtained. In Table 3, the parameter values of each solution $\mathbf{x} \in \mathbf{X}^{nom}$ and the evaluation of the objective functions $f_1(\mathbf{x}, \mathbf{p}^0)$ and $f_2(\mathbf{x}, \mathbf{p}^0)$ that constitute the Pareto front $\mathbf{F}^{nom} = \boldsymbol{f}(\mathbf{X}^{nom}, \mathbf{p}^0)$ are presented. In Fig. 20, the front $\mathbf{F}^{nom}$ is

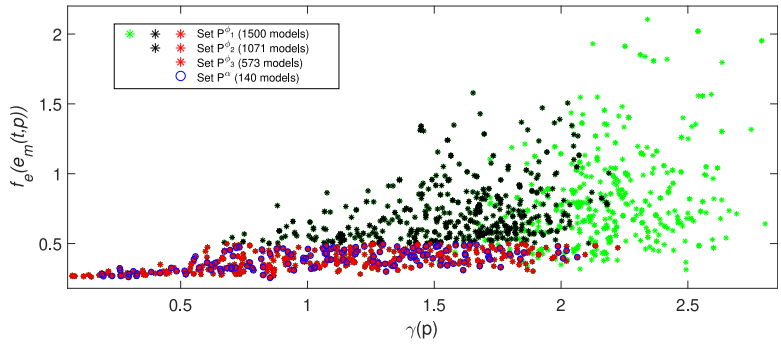

Fig. 15. Design process of set $\mathbf{P}^{\alpha}$ from set $\mathbf{P}^{\phi_1}$.

Table 3
Control parameter results obtained for the Pareto set of solutions $\mathbf{X}^{nom}$.

$\mathbf{X}^{nom}$	K_{c1}	T_{i1}	K_{c2}	T_{i2}	$f_1(\mathbf{x},\mathbf{p}^0)$	$f_2(\mathbf{x},\mathbf{p}^0)$	$f_{1_{max}}(\mathbf{x},\mathbf{P}^{\alpha})$	$f_{2_{max}}(\mathbf{x},\mathbf{P}^{\alpha})$
$\mathbf{x}^1$	−0.69	40.32	−4.90	64.19	0.165	6.9e−3	0.190	8.7e−3
$\mathbf{x}^2$	−0.72	49.18	−4.12	69.14	0.200	6.3e−3	0.227	8.1e−3
$\mathbf{x}^3$	−0.88	62.72	−3.73	76.78	0.223	6.3e−3	0.252	8.0e−3
$\mathbf{x}^4$	−0.90	59.68	−4.07	61.83	0.189	6.5e−3	0.212	8.4e−3
$\mathbf{x}^5$	−0.60	58.79	−4.30	75.72	0.258	6.2e−3	0.277	7.2e−3
$\mathbf{x}^6$	−0.86	113.56	−3.95	112.88	0.365	6.0e−3	0.396	7.1e−3
$\mathbf{x}^7$	−1.01	35.54	−6.98	57.04	0.124	11.5e−3	0.151	13.9e−3
$\mathbf{x}^8$	−0.78	42.62	−4.50	49.45	0.150	7.2e−3	0.177	9.5e−3
$\mathbf{x}^9$	−0.73	45.07	−4.42	66.84	0.180	6.5e−3	0.207	8.5e−3
$\mathbf{x}^{10}$	−0.88	51.47	−4.70	71.75	0.175	6.7e−3	0.203	8.7e−3
$\mathbf{x}^{11}$	−0.90	47.16	−5.59	52.30	0.144	7.9e−3	0.169	10.0e−3

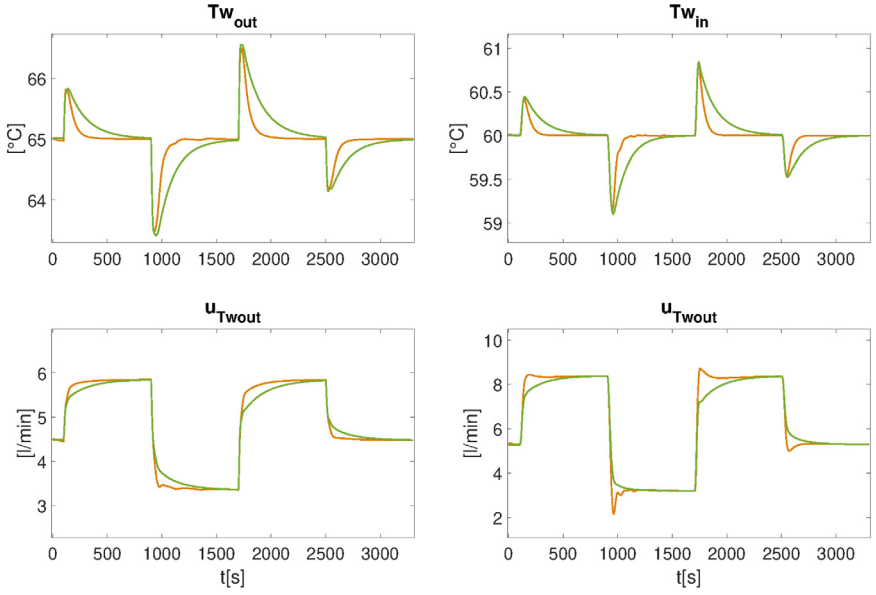

Fig. 16. Dynamic response of the system controlled by $\mathbf{x}^6 \in \mathbf{X}^{nom}$(green) and $\mathbf{x}^{11} \in \mathbf{X}^{nom}$(orange).

represented by red squares (some solutions are located outside the scale of the graph). In addition, Table 3 also shows the evaluation of robustness indices $f_{1_{max}}(\mathbf{x},\mathbf{P}^{\alpha})$ and $f_{2_{max}}(\mathbf{x},\mathbf{P}^{\alpha})$ which are further analyzed in Section 6.

To contrast the performance of the solutions obtained in set $\mathbf{X}^{nom}$, Fig. 16 shows the system response controlled by solutions located at the extremes of the front $\mathbf{F}^{nom}$. The green function represents the performance of solution $\mathbf{x}^6 \in \mathbf{X}^{nom}$ (good performance in f_2, poor performance in f_1). The orange function represents the performance of the solution $\mathbf{x}^{11} \in \mathbf{X}^{nom}$ (good performance in f_1, poor performance in f_2). The performance of the remaining solutions with a better balance for both objectives takes place between these two functions.

- *Step 3.2*
  By using the set of models, $\mathbf{P}^{\alpha}$ obtained in Stage 2, an objective degradation analysis is carried out for each controller in $\mathbf{X}^{nom}$. Fig. 17 shows the analysis for the controller $\mathbf{x}^4 \in \mathbf{X}^{nom}$, which is a solution with a good balance between objectives $f_1(\mathbf{x},\mathbf{p}^0)$ and $f_2(\mathbf{x},\mathbf{p}^0)$ (see Table 3). In this figure, the nominal model $\boldsymbol{f}(\mathbf{x}^4,\mathbf{p}^0)$ is represented by a red dot and the objective degradation due to uncertainties $\boldsymbol{f}(\mathbf{x}^4,\mathbf{P}^{\alpha})$ is represented by green circles. Fig. 18 shows the system response controlled by solution $\mathbf{x}^4 \in \mathbf{X}^{nom}$. The red line represents the evaluation of the nominal model $\mathbf{p}^0$, and the blue area represents the degradation of the performance under the evaluation of the uncertainty framework $\mathbf{P}^{\alpha}$.
- *Step 3.3*

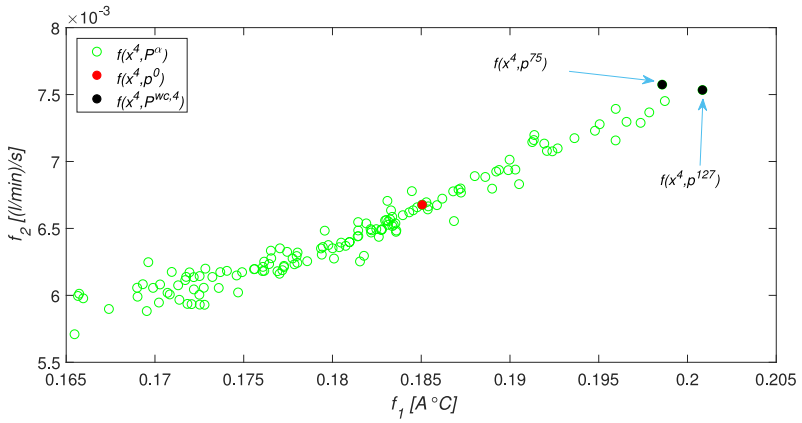

Fig. 17. Identification of worst-case models in the objective degradation analysis of controller $\mathbf{x}^4 \in \mathbf{X}^{nom}$ due to parameter uncertainties $\mathbf{P}^{\alpha}$.

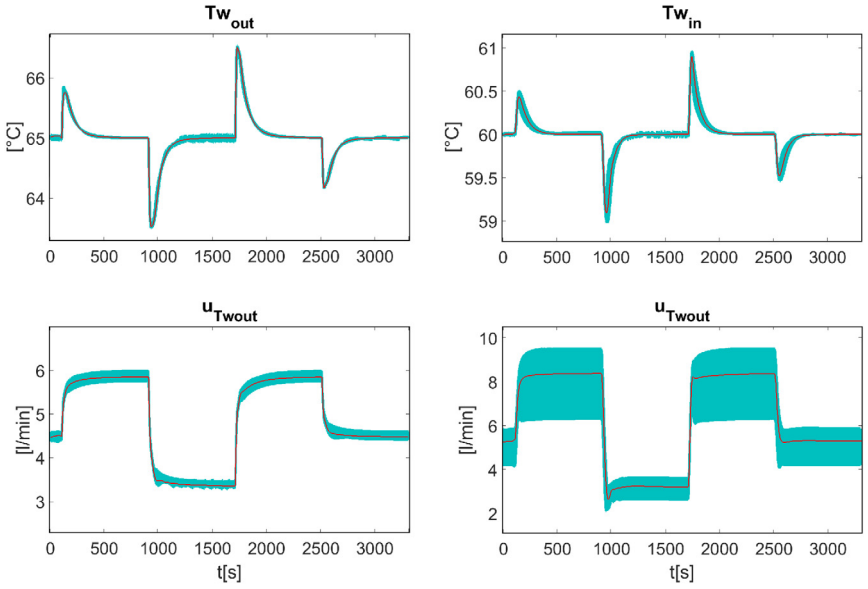

Fig. 18. Dynamic response of the system controlled by $\mathbf{x}^4 \in \mathbf{X}^{nom}$ under nominal model $\mathbf{p}^0$ (red) and under uncertainties $\mathbf{P}^{\alpha}$ (blue zone).

From the degradation analysis displayed in the previous step, we define the subset $\mathbf{P}^{\beta} \subset \mathbf{P}^{\alpha}$ under the worst-case index as required by the formulation defined in Eqs. (29)–(37) based on the model characterization strategy shown in Fig. 5 using the Pareto dominance concept. In Fig. 17 we show the identification of the worst-case models found in the degradation analysis of the controller $\mathbf{x}^4 \in \mathbf{X}^{nom}$. Where the black dots represent the set of worst-case models $\mathbf{P}^{wc,4} = \{\mathbf{p}^{75}, \mathbf{p}^{127}\}$ determined in this analysis. This same approach is followed to define the sets $\mathbf{P}^{wc,t}$ (such that $t = \{1, \ldots, 11\}$) of the remaining controllers in $\mathbf{X}^{nom}$. The result of this process is set $\mathbf{P}^{\beta} = \{\mathbf{P}^{wc,1} \cup \mathbf{P}^{wc,1} \cup, \ldots, \mathbf{P}^{wc,11}\}$, which is finally constituted by the models $\{\mathbf{p}^{37}, \mathbf{p}^{41}, \mathbf{p}^{50}, \mathbf{p}^{75}, \mathbf{p}^{99}, \mathbf{p}^{127}, \mathbf{p}^{133}, \mathbf{p}^{134}, \mathbf{p}^{138}\} \in \mathbf{P}^{\alpha}$.

Table 5 shows the recurrence (number of times) that these models have been identified in the degradation analysis $\boldsymbol{f}(\mathbf{X}^{nom}, \mathbf{P}^{\alpha})$ using the worst-case concept. For example, model $\mathbf{p}^{127}$ was defined as the worst-case in 9 of the 11 controllers analyzed, while models $\{\mathbf{p}^{41}, \mathbf{p}^{50}, \mathbf{p}^{99}, \mathbf{p}^{133}, \mathbf{p}^{134}\}$ were only identified for one single controller.

6. Discussion of results

This section focuses on analyzing the results obtained after solving the robust optimization problem stated in Section 4 and emphasizes the relevance of formulating an appropriate parameter uncertainty modeling.

6.1. Robust controller analysis

By using the uncertainty set $\mathbf{P}^{\beta}$ defined in Section 5 and solving the Eqs. (29)–(37), the set of controllers $\mathbf{X}^{wc} = \{\mathbf{x}^1_{wc}, \mathbf{x}^2_{wc}, \ldots, \mathbf{x}^{12}_{wc}\}$ is obtained. This set has good robustness characteristics (evaluated as worst-case) without excessive loss of performance in the nominal case. To carry out the optimization process, the evolutionary algorithm evMOGA (Martínez et al., 2009) was used. In Table 4, the parameter values of each solution $\mathbf{x} \in \mathbf{X}^{wc}$ are presented. Fig. 19 shows the system response controlled by solution $\mathbf{x}^4 \in \mathbf{X}^{wc}$ (solution with a good balance between objectives $f_{1_{max}}$ and $f_{2_{max}}$) under the evaluation of the uncertainty framework $\mathbf{P}^{\alpha}$. To analyze the performance and robustness of the entire set of solutions, Table 4 also presents the evaluation of the objective functions $f_1(\mathbf{x}, \mathbf{p}^0)$ and $f_2(\mathbf{x}, \mathbf{p}^0)$, and the evaluation of the robustness index $f_{1_{max}}(\mathbf{x}, \mathbf{P}^{\alpha})$ and $f_{2_{max}}(\mathbf{x}, \mathbf{P}^{\alpha})$ calculated under consideration of the uncertainty framework $\mathbf{P}^{\alpha}$. The same index $f_{max}(\mathbf{x}, \mathbf{P}^{\alpha})$ is also calculated for the set of solutions $\mathbf{X}^{nom}$ and shown in Table 3.

A comparative analysis of control performance in the objective space between the sets $\mathbf{X}^{nom}$ and $\mathbf{X}^{wc}$ is shown in Fig. 20. This analysis contrasts two aspects; one is the performance of the controllers on the nominal model $\boldsymbol{f}(\mathbf{x}, \mathbf{p}^0)$, represented by red squares and black stars for

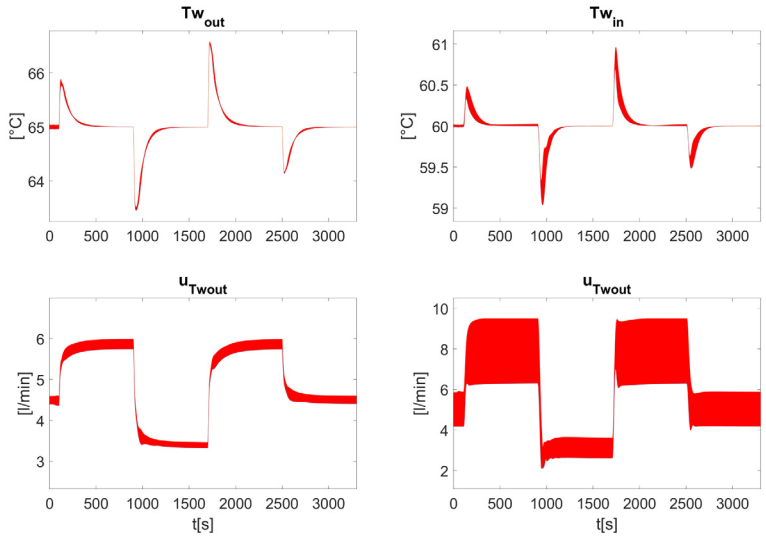

Fig. 19. Dynamic response of the system controlled by $\mathbf{x}^4 \in \mathbf{X}^{wc}$ under uncertainties $\mathbf{P}^{\alpha}$.

Table 4
Control parameter results obtained for the set of solutions $\mathbf{X}^{wc}$.

$\mathbf{X}^{wc}$	K_{c1}	T_{i1}	K_{c2}	T_{i2}	$f_1(\mathbf{x},\mathbf{p^0})$	$f_2(\mathbf{x},\mathbf{p^0})$	$f_{1_{max}}(\mathbf{x},\mathbf{P}^{\alpha})$	$f_{2_{max}}(\mathbf{x},\mathbf{P}^{\alpha})$
$\mathbf{x}^1$	−0.86	113.56	−3.95	112.88	0.365	6.0e−3	0.396	7.1e−3
$\mathbf{x}^2$	−0.71	44.88	−5.72	44.33	0.158	8.0e−3	0.176	8.8e−3
$\mathbf{x}^3$	−0.68	42.85	−4.66	47.96	0.163	7.3e−3	0.181	8.4e−3
$\mathbf{x}^4$	−0.83	55.09	−4.53	62.16	0.185	6.7e−3	0.200	7.6e−3
$\mathbf{x}^5$	−0.55	47.34	−4.98	69.36	0.223	6.4e−3	0.238	7.3e−3
$\mathbf{x}^6$	−0.75	45.46	−6.25	47.49	0.152	8.0e−3	0.170	9.2e−3
$\mathbf{x}^7$	−1.01	35.54	−6.98	57.04	0.124	11.5e−3	0.151	13.9e−3
$\mathbf{x}^8$	−0.79	50.00	−5.36	66.08	0.172	7.5e−3	0.189	8.2e−3
$\mathbf{x}^9$	−0.81	45.79	−6.82	56.55	0.149	8.1e−3	0.165	9.9e−3
$\mathbf{x}^{10}$	−0.57	43.02	−4.78	64.19	0.199	6.5e−3	0.215	7.5e−3
$\mathbf{x}^{11}$	−0.67	43.71	−4.80	61.56	0.178	6.8e−3	0.194	7.7e−3
$\mathbf{x}^{12}$	−0.56	59.12	−4.84	68.24	0.257	6.3e−3	0.273	7.2e−3

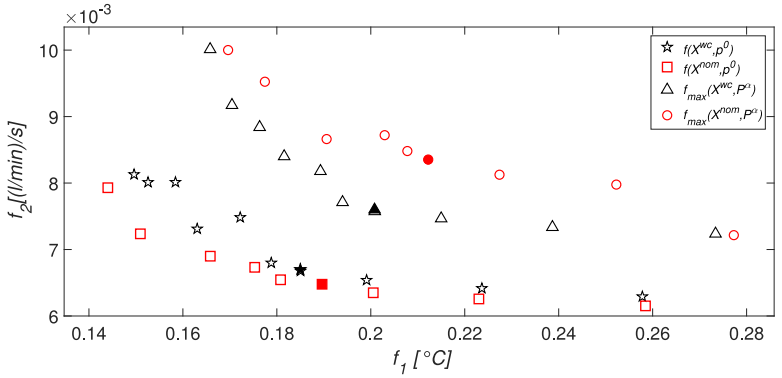

Fig. 20. Comparison between the set of controllers $\mathbf{X}^{nom}$ and $\mathbf{X}^{wc}$ under the nominal model and the worst-case index.

the sets $\mathbf{X}^{nom}$ and $\mathbf{X}^{wc}$ respectively. The second is the robustness to the uncertainty framework $\mathbf{P}^{\alpha}$ evaluated by the worst-case index $\boldsymbol{f}_{max}(\mathbf{x},\mathbf{P}^{\alpha})$ and represented by red circles and black triangles for the sets $\mathbf{X}^{nom}$ and $\mathbf{X}^{wc}$ respectively. In this Figure, some controllers are located outside the scale. The evaluation of all solutions shown in this figure for sets $\mathbf{X}^{nom}$ and $\mathbf{X}^{wc}$ have been presented above in Tables 3 and 4.

From this analysis, it can be noted that there is a slight loss of performance of set $\mathbf{X}^{wc}$ compared to $\mathbf{X}^{nom}$ in the nominal model $\mathbf{p^0}$. If only the nominal scenario is considered, solutions $\mathbf{X}^{wc}$ would be identified as sub-optimal. However, the set $\mathbf{X}^{wc}$ shows an evident improvement in the minimization of the worst-case index, and there are no solutions of set $\mathbf{X}^{nom}$ that can dominate them. Fig. 20 highlights the solutions $\mathbf{x}^4 \in \mathbf{X}^{nom}$ and $\mathbf{x}^4 \in \mathbf{X}^{wc}$ used as a reference in the simulations of the system performance under uncertainties shown in Figs. 18 and 19. Functions $\boldsymbol{f}(\mathbf{x},\mathbf{p}^0)$ and $\boldsymbol{f}_{max}(\mathbf{x},\mathbf{P}^{\alpha})$ for solution $\mathbf{x}^4 \in \mathbf{X}^{nom}$ are denoted by a solid red square and a solid red circle respectively. The same functions are marked for solution $\mathbf{x}^4 \in \mathbf{X}^{wc}$ by a solid black star and a solid black triangle respectively. The selection of two solutions with an equal balance of objectives is intended to make the performance comparison as fair as possible. In Fig. 22, a comparison between the system responses shown in Figs. 18 and 19 for these two solutions is provided. The red area representing the performance of the controller $\mathbf{x}^4 \in \mathbf{X}^{wc}$ under uncertainties exhibits less degradation than the red area (controller $\mathbf{x}^4 \in \mathbf{X}^{nom}$), particularly in the steady-state zones.

Using the set $\mathbf{X}^{\mathbf{wc}}$ as reference controllers, we again perform the model characterization process shown in Fig. 17 and described in step

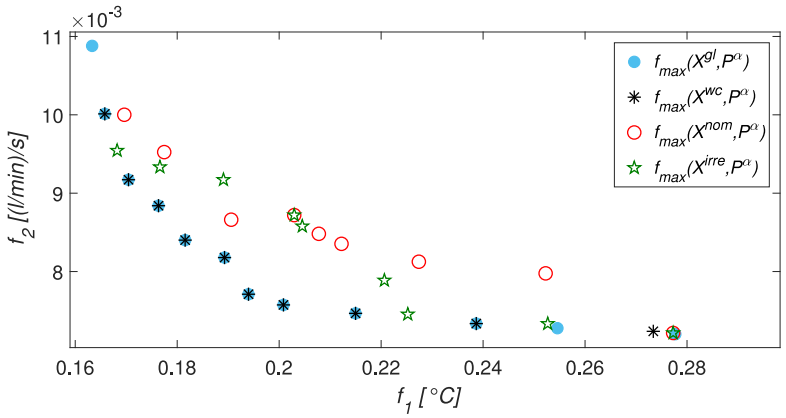

Fig. 21. Robustness comparison between sets $\mathbf{X}^{nom}$, $\mathbf{X}^{wc}$, $\mathbf{X}^{ran}$ and $\mathbf{X}^{gl}$ under the worst-case index.

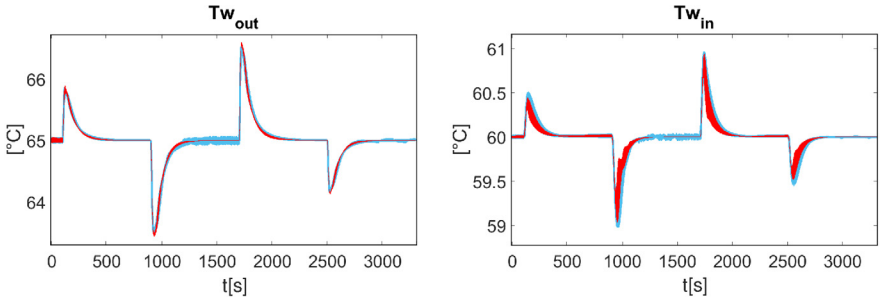

Fig. 22. Comparison between the dynamic response of the system under uncertainty $\mathbf{P}^{\alpha}$ controlled by $\mathbf{x}^4 \in \mathbf{X}^{nom}$ (blue) and $\mathbf{x}^4 \in \mathbf{X}^{wc}$ (red).

Table 5
Recurrence of worst-case model identification in the degradation analysis $f(\mathbf{X}^{nom}, \mathbf{P}^{\alpha})$ and $f(\mathbf{X}^{wc}, \mathbf{P}^{\alpha})$.

Recurrence	Worst-case models identified in $f(\mathbf{X}^{nom}, \mathbf{P}^{\alpha})$	Worst-case models identified in $f(\mathbf{X}^{wc}, \mathbf{P}^{\alpha})$
11 times	none	$\mathbf{p}^{127}$
9 times	$\mathbf{p}^{127}$	none
5 times	$\mathbf{p}^{75}$	$\mathbf{p}^{75}$
4 times	none	$\mathbf{p}^{133}$, $\mathbf{p}^{138}$
3 times	none	$\mathbf{p}^{37}$, $\mathbf{p}^{134}$
2 times	$\mathbf{p}^{37}$, $\mathbf{p}^{138}$	$\mathbf{p}^{50}$
1 time	$\mathbf{p}^{41}$, $\mathbf{p}^{50}$, $\mathbf{p}^{99}$, $\mathbf{p}^{133}$, $\mathbf{p}^{134}$	$\mathbf{p}^{41}$, $\mathbf{p}^{99}$, $\mathbf{p}^{109}$

3.3 of the methodology. The set of worst-case models identified in the degradation analysis $f(\mathbf{X}^{\mathbf{wc}}, \mathbf{P}^{\alpha})$ is $\{\mathbf{p}^{37}, \mathbf{p}^{41}, \mathbf{p}^{50}, \mathbf{p}^{75}, \mathbf{p}^{99}, \mathbf{p}^{109}, \mathbf{p}^{127}, \mathbf{p}^{133}, \mathbf{p}^{134}, \mathbf{p}^{138}\} \in \mathbf{P}^{\alpha}$. The recurrence of model identification in the degradation analysis for all the controllers in $\mathbf{X}^{\mathbf{wc}}$ is presented in the second column of Table 5. Based on this analysis, we can observe that the worst-case models identified in the degradation analysis $f(\mathbf{X}^{nom}, \mathbf{P}^{\alpha})$ with the highest recurrence coincide with the worst-case models of the highest recurrence identified in the degradation analysis $f(\mathbf{X}^{wc}, \mathbf{P}^{\alpha})$. This fact is the indicator to confirm that the set of models used to address the robust control design has been adequately selected since the characterization of the uncertainty models with different reference controllers provides similar results.

6.2. Repercussion of appropriate uncertainty modeling on robust control design

To highlight the importance of defining a good set that should adequately represent the global set showing the robustness characteristics to be evaluated, the problem of Eqs. (29)–(37) is again solved under the worst-case minimization for the following uncertainty cases: (a) the uncertainty framework $\mathbf{P}^{\alpha}$ and (b) the low relevant model set $\mathbf{P}^{ran}$.

Therefore, we will see that $\mathbf{P}^{\beta}$ clearly shows the robustness of $\mathbf{P}^{\alpha}$ and that a random $\mathbf{P}^{\alpha}$ sample of the same size as $\mathbf{P}^{\beta}$ is not good for robustness assessment.

Approach (a) consists of solving the robust control problem under the consideration of the set $\mathbf{P}^{\alpha}$, which represents the entire uncertainty framework of the system. Approach (b) formulates the robust control problem under a subset of nine randomly models selected from $\mathbf{P}^{\alpha}$ (same size than $\mathbf{P}^{\beta}$), such that $\mathbf{p} \notin \mathbf{P}^{wc}$.

As a result of the control tuning under the approaches (a) and (b), the sets of controllers $\mathbf{X}^{gl}$ and $\mathbf{X}^{ran}$ are obtained respectively. Fig. 21 presents a robustness comparison between the sets $\mathbf{X}^{nom}$, $\mathbf{X}^{wc}$, $\mathbf{X}^{gl}$ and $\mathbf{X}^{ran}$ under the worst-case index when the uncertainty framework $\mathbf{P}^{\alpha}$ is considered. From this analysis, we notice that the sets of solutions $\mathbf{X}^{nom}$ (red circles) exhibit the worst evaluation of the worst-case index. The sets $\mathbf{X}^{gl}$ (blue dots) and $\mathbf{X}^{wc}$ (black asterisks) show the best minimization of this index. Some controllers of set $\mathbf{X}^{ran}$ (green stars) minimize the index worst-case with respect to $\mathbf{X}^{nom}$, but it is not even close to the result exhibited by $\mathbf{X}^{wc}$.

Since the set $\mathbf{X}^{wc}$ manages to minimize the worst-case index almost as much as $\mathbf{X}^{gl}$, it provides evidence confirming the excellent representative quality of the set of models $\mathbf{P}^{\beta}$ regarding the uncertainty framework $\mathbf{P}^{\alpha}$ for addressing the robust control problem. In addition, the fact that the set $\mathbf{X}^{ran}$ shows an intermediate performance between $\mathbf{X}^{nom}$ and $\mathbf{X}^{wc}$ suggests that an inappropriate definition of the uncertainty models used for formulating the control problem may lead to an inadequate tuning of robust controllers.

6.3. Computational cost associated with the uncertainty modeling methodology

The simulation cost is the most significant computational cost involved in applying the methodology for uncertainty modeling. Table 6 summarizes the sets of models used and the representation of the computational cost in the modeling process. Stages 1 and 2 are necessary

Table 6
Comparison of the uncertainty sets used in the modeling process.

Set	Set size (number of models)	Computational cost (number of simulations)
$\mathbb{P}$	589	589
$\mathbf{P}^{\phi_1}$	1500	No simulations
$\mathbf{P}^{\phi_2}$	1071	1071
$\mathbf{P}^{\phi_3}$	573	No simulations
$\mathbf{P}^{\alpha}$	140	1540
$\mathbf{P}^{\beta}$	9	No simulations

Table 7
Summary of the computational cost involved in processing each set of models in uncertainty modeling.

Set	Set size (number of controllers)	Computational cost (number of simulations)
$\mathbf{X}^{nom}$	11	20000
$\mathbf{X}^{wc}$	12	201540
$\mathbf{X}^{gl}$	14	2800000

to define the framework $\mathbf{P}^{\alpha}$ under a representative uncertainty domain that should not lead to conservative controllers. These stages involve the simulation of the sets $\mathbb{P}$ and $\mathbf{P}^{\phi_2}$ in an open loop, which represents a cost of 589 and 1071 simulations respectively. Stage 3 is used to define the set of models $\mathbf{P}^{\beta}$ that formulates the robust control problem. This stage involves the simulation of set $\mathbf{P}^{\alpha}$ for each controller defined in $\mathbf{X}^{nom}$ in closed loop. This process represents 1540 simulations. Based on this, the total simulation cost for defining the uncertainty framework $\mathbf{P}^{\alpha}$ is 1660 simulations, and the cost for defining the set $\mathbf{P}^{\beta}$ from $\mathbf{P}^{\alpha}$ is 1540 simulations.

For the computational cost involved in the robust control problem, we present in Table 7 a comparison between using the sets $\mathbf{P}^{\alpha}$ and $\mathbf{P}^{\beta}$ in the optimization process. To make the comparison as fair as possible, the evolutionary algorithm evMOGA (Martínez et al., 2009) was used under the same configuration (same population size, same generations, etc.). The optimization process to determine X^{nom} under the nominal model $\mathbf{p}^0$ was carried out with only 20,000 evaluations of the objective function. The optimization process to determine X^{gl} under the uncertainty framework $\mathbf{P}^{\alpha}$ (140 models) needed 2,800,000 evaluations. The computational cost to determine X^{wc} under the set $\mathbf{P}^{\beta}$ (nine models) involved 201,540 evaluations. This cost includes the 20,000 evaluations needed to determine X^{nom}, the 1540 evaluations representing the cost of the degradation analyses used to determine $\mathbf{P}^{\beta}$ from $\mathbf{P}^{\alpha}$ and 180,000 evaluations of the optimization process to solve the robust control problem. As can be seen, tackling the robust control problem under the set $\mathbf{P}^{\beta}$ represents an approximate cost reduction of 92.8% compared to using $\mathbf{P}^{\alpha}$ in the optimization process.

7. Conclusions

Formulating a robust control problem usually requires defining the set of uncertainty scenarios facing the system. When dealing with non-linear systems involving many parameters, inappropriate modeling of uncertainties may lead to a highly conservative performance in the control design. To address this problem, this paper presents a new methodology for modeling parameter uncertainty. This modeling is distinguished by representing a computationally feasible cost and limiting conservatism to uncertainty cases with higher probabilities. The novelty of this process consists in using the multiobjective space to identify a set of scenarios with properties that are highly relevant for the robust control design. A minimization strategy for robust controller tuning must be pre-established. The advantages of this methodology enable the designer to define a region of interest in the domain of uncertainties and obtain a reduced computational cost representation. Its application is not restricted to the number of parameters in which uncertainties are considered or the use of linear or nonlinear models.

To describe the methodology, the temperature control design of a PEMFC system is presented in this work. This approach is used to minimize the worst-case index within an uncertainty framework defined for this system. The dynamic model has been identified and experimentally validated in Navarro et al. (2019), Ferrando et al. (2020). In addition, a multiloop PID design under a multiobjective optimization approach to control the temperature of the PEMFC stack is addressed in Gimenez et al. (2020). The results of these papers suggest exploring a robust control approach due to the presence of uncertainties in the model parameters.

After applying our methodology for uncertainty modeling, two sets of models are defined. The first is the uncertainty framework of the system $\mathbf{P}^{\alpha}$ with 140 models, the second is the set $\mathbf{P}^{\beta}$ with nine models. This second set is a representative sample of $\mathbf{P}^{\alpha}$ representing 7.2% of the computational cost and addresses the robust control problem under worst-case minimization.

A robust control design is carried out while considering the set of models $\mathbf{P}^{\beta}$. Theoretical results obtained in simulations (as can be seen in Figs. 19–22) show that the robust controllers obtained attenuate the effect of uncertainties and despite a slight performance loss on the nominal model, present an evident minimization of the worst-case index compared to non-robust controllers. Moreover, based on the performance analysis of robust controllers, we can verify that $\mathbf{P}^{\beta}$ is an appropriate representation of the uncertainty framework $\mathbf{P}^{\alpha}$ according to the following aspects: (1) the characterization process of the worst-case models in $\mathbf{P}^{\alpha}$ provides results with a high percentage of similarity when using $\mathbf{X}^{nom}$ or $\mathbf{X}^{wc}$ as reference controllers; (2) the minimization degree of the worst-case index achieved by $\mathbf{X}^{wc}$ is similar to that exhibited by $\mathbf{X}^{gl}$, which was tuned after solving the robust control problem under the consideration of the uncertainty framework $\mathbf{P}^{\alpha}$. From these results, it is evidenced that model characterization in the objective space represents a very efficient approach for defining highly representative uncertainty models.

Finally, the results obtained provide a basis for future work and lines of research: (1) experimental validation of the robust control design achieved in this work in the PEMFC system; (2) optimization of the control design by addressing various concepts and strategies (such as predictive control, nonlinear methods, and fuzzy control) for improving current system performance; (3) Uncertainty modeling and robust control design under the minimization approach for different robustness indices.

CRediT authorship contribution statement

U. Veyna: Conceptualization, Methodology, Software, Validation, Writing – original draft. **X. Blasco:** Investigation, Supervision, Writing – review & editing, Funding acquisition. **J.M. Herrero:** Methodology, Investigation, Supervision, Writing – review & editing, Funding acquisition. **A. Pajares:** Investigation, Validation, Writing – review & editing.

Declaration of competing interest

The authors declare that they have no known competing financial interests or personal relationships that could have appeared to influence the work reported in this paper.

Data availability

Data will be made available on request.

Acknowledgments

This work was supported in part by grant PID2021-124908NB-I00 founded by MCIN/AEI/10.13039/501100011033 and by "ERDF A way of making Europe"; by grant SP20200109 (PAID-10-20) funded by Universitat Politècnica de València; and by grant PRE2019-087579 funded by MCIN/AEI/10.13039/501100011033 and by "ESF Investing in your future"; and by the Generalitat Valenciana regional government through project CIAICO/2021/064. Funding for open access charge: CRUE-Universitat Politècnica de València.

References

Ackermann, J., 1985. Multi-model approaches to robust control system design. IFAC Proc. Vol. 18 (3), 1–6. http://dx.doi.org/10.1016/B978-0-08-032575-0.50006-0, IFAC Workshop on Model Error Concepts and Compensation, Boston, USA, 17-18 June.

Assis, J., Machado-Coelho, T., Soares, G., Mendes, M., 2018. Robust evolutionary optimization algorithm for multi-objective environmental/economic dispatch problem with uncertainties. http://dx.doi.org/10.1109/CEC.2018.8477923.

Ben-Tal, A., And, T., Nemirovski, A., 1998. Robust convex optimization. Math. Oper. Res. - MOR 23, http://dx.doi.org/10.1287/moor.23.4.769.

Ben-Tal, A., Nemirovski, A., 2002. Robust optimization-methodology and applications. Math. Program. 92, 453–480. http://dx.doi.org/10.1007/s101070100286.

Bernal, E., Lagunes, M., Castillo, O., Soria, J., Valdez, F., 2020. Optimization of type-2 fuzzy logic controller design using the GSO and FA algorithms. Int. J. Fuzzy Syst. 23, http://dx.doi.org/10.1007/s40815-020-00976-w.

Bertsimas, D., Brown, D., Caramanis, C., 2010. Theory and applications of robust optimization. SIAM Rev. 53, http://dx.doi.org/10.1137/080734510.

Bertsimas, D., Sim, M., 2004. The price of robustness. Oper. Res. 52, 35–53. http://dx.doi.org/10.1287/opre.1030.0065.

Borgonovo, E., 2010. A methodology for determining interactions in probabilistic safety assessment models by varying one parameter at a time. Risk Anal. : Official Publ. Soc. Risk Anal. 30, 385–399. http://dx.doi.org/10.1111/j.1539-6924.2010.01372.x.

Cavaliere, V., Cioffi, M., Formisano, A., Martone, R., 2003. Robust design of high field magnets through Monte Carlo analysis. COMPEL 22, 589–602. http://dx.doi.org/10.1108/03321640310475056.

Chen, T., Babanin, A., Muhammad, A., Chapron, B., Chen, C., 2020. Modified evolved bat algorithm of fuzzy optimal control for complex nonlinear systems. Rom. J. Inf. Sci. Technol. 23, T28–T40.

Cuevas, F., Castillo, O., Cortés-Antonio, P., 2022. Optimal setting of membership functions for interval type-2 fuzzy tracking controllers using a shark smell metaheuristic algorithm. Int. J. Fuzzy Syst. 24, 799–822.

Ferrando, A., Blasco, X., Herrero, J., Salcedo, J., 2020. Analyzing the nearly optimal solutions in a multi-objective optimization approach for the multivariable nonlinear identification of a PEM fuel cell cooling system. IEEE Access PP, 1. http://dx.doi.org/10.1109/ACCESS.2020.3003741.

Freer, J.E., Beven, K.J., Ambroise, B., 1996. Bayesian estimation of uncertainty in runoff prediction and the value of data: An application of the GLUE approach. Water Resour. Res. 32, 2161–2173.

Gimenez, S., Herrero, J., Blasco, X., Fernandez, R., 2020. Design and experimental validation of the temperature control of a PEMFC stack by applying multiobjective optimization. IEEE Access 8, 183324–183343. http://dx.doi.org/10.1109/ACCESS.2020.3029321.

Godfrey, K., 2000. Identification of parametric models from experimental data [book review]. IEEE Trans. Automat. Control 44, 2321–2322. http://dx.doi.org/10.1109/TAC.1999.811220.

Gorinevsky, D., Stein, G., 2003. Structured uncertainty analysis of robust stability for multidimensional array systems. IEEE Trans. Automat. Control 48 (9), 1557–1568. http://dx.doi.org/10.1109/TAC.2003.816980.

Gorissen, B., Yanıkoğlu, İ., den Hertog, D., 2015. A practical guide to robust optimization. Omega 53, 124–137. http://dx.doi.org/10.1016/j.omega.2014.12.006.

Helton, J., 1993. Uncertainty and sensitivity analysis techniques for use in performance assessment for radioactive waste disposal. Reliab. Eng. Syst. Saf. 42, 327–367. http://dx.doi.org/10.1016/0951-8320(93)90097-I.

Huang, L., Chen, J., Liu, Z., Becherif, M., 2018. Adaptive thermal control for PEMFC systems with guaranteed performance. Int. J. Hydrogen Energy 43, http://dx.doi.org/10.1016/j.ijhydene.2017.12.121.

Huilcapi, V., Blasco, X., Herrero, J.M., Reynoso-Meza, G., 2019. A loop pairing method for multivariable control systems under a multi-objective optimization approach. IEEE Access 7, 81994–82014. http://dx.doi.org/10.1109/ACCESS.2019.2923654.

Ibrahim, M., Al-Sobhi, S., Mukherjee, R., Alnouss, A., 2019. Impact of sampling technique on the performance of surrogate models generated with artificial neural network (ANN): A case study for a natural gas stabilization unit. Energies 12, http://dx.doi.org/10.3390/en12101906.

Ide, J., Schöbel, A., 2016. Robustness for uncertain multi-objective optimization: A survey and analysis of different concepts. OR Spectrum 38, http://dx.doi.org/10.1007/s00291-015-0418-7.

Jahanshahi, H., Yousefpour, A., Munoz-Pacheco, J.M., Moroz, I., Wei, Z., Castillo, O., 2020. A new multi-stable fractional-order four-dimensional system with self-excited and hidden chaotic attractors: Dynamic analysis and adaptive synchronization using a novel fuzzy adaptive sliding mode control method. Appl. Soft Comput. 87, 105943. http://dx.doi.org/10.1016/j.asoc.2019.105943.

Johansen, T.A., Murray-Smith, R., 1997. The operating regime approach to nonlinear modelling and control. In: Murray-Smith, R., Johansen, T.A. (Eds.), Multiple Model Approaches to Modelling and Control. Taylor and Francis, London, pp. 3–72, chapter 1.

Kamali, M., Ponnambalam, K., Soulis, E., 2007. Integration of surrogate optimization and PCA for calibration of hydrologic models, a WATCLASS case study. In: Conference Proceedings - IEEE International Conference on Systems, Man and Cybernetics. pp. 2733–2737. http://dx.doi.org/10.1109/ICSMC.2007.4414073.

Kristiansson, B., Lennartson, B., 2002. Robust and optimal tuning of PI and PID controllers. Control Theory Appl., IEE Proc. 149, 17–25. http://dx.doi.org/10.1049/ip-cta:20020088.

Kuo, T., Huang, Y., Chen, C., Chang, C., 2008. Adaptive sliding mode control with PID tuning for uncertain systems. Eng. Lett. 16, 311–315.

Maitra, S., Yan, J., 2008. Principle component analysis and partial least squares: Two dimension reduction techniques for regression.

Marler, R., Arora, J., 2004. Survey of multi-objective optimization methods for engineering. Struct. Multidiscip. Optim. 26, 369–395. http://dx.doi.org/10.1007/s00158-003-0368-6.

Martínez, M., Herrero, J., Sanchis, J., Blasco, X., Garcia-Nieto Rodriguez, S., 2009. Applied Pareto multi-objective optimization by stochastic solvers. Eng. Appl. Artif. Intell. 22, 455–465. http://dx.doi.org/10.1016/j.engappai.2008.10.018.

Mckay, M., Beckman, R., Conover, W., 1979. A comparison of three methods for selecting vales of input variables in the analysis of output from a computer code. Technometrics 21, 239–245. http://dx.doi.org/10.1080/00401706.1979.10489755.

Miettinen, K., Hakanen, J., Podkopaev, D., 2016. Interactive Nonlinear Multiobjective Optimization Methods, Vol. 233. pp. 927–976. http://dx.doi.org/10.1007/978-1-4939-3094-4_22.

Navarro, S., Herrero, J., Blasco, X., Simarro, R., 2019. Control-oriented modeling of the cooling process of a PEMFC-based μ-CHP system. IEEE Access PP, 1. http://dx.doi.org/10.1109/ACCESS.2019.2928632.

Ogata, K., 2010.. Ingeniería de Control Moderna, fifth ed. Pearson Educación, Madrid.

Pianosi, F., Beven, K., Freer, J., Hall, J., Rougier, J., Stephenson, D., Wagener, T., 2016. Sensitivity analysis of environmental models: A systematic review with practical workflow. Environ. Model. Softw. 79, 214–232. http://dx.doi.org/10.1016/j.envsoft.2016.02.008.

Puschke, J., Zubov, A., Kosek, J., Mitsos, A., 2016. Multi-model approach based on parametric sensitivities – A heuristic approximation for dynamic optimization of semi-batch processes with parametric uncertainties. Comput. Chem. Eng. 98, http://dx.doi.org/10.1016/j.compchemeng.2016.12.004.

Shang, C., Huang, X., You, F., 2017. Data-driven robust optimization based on kernel learning. Comput. Chem. Eng. 106, http://dx.doi.org/10.1016/j.compchemeng.2017.07.004.

Slupphaug, O., Foss, B.A., 2000. Multi-model based uncertainty and robust control design. IFAC Proc. Vol. 33 (10), 45–50. http://dx.doi.org/10.1016/S1474-6670(17)38516-6, IFAC Symposium on Advanced Control of Chemical Processes 2000, Pisa, Italy, 14-16 June 2000.

Soyster, A., 1973. Technical note–convex programming with set-inclusive constraints and applications to inexact linear programming. Oper. Res. 21, 1154–1157. http://dx.doi.org/10.1287/opre.21.5.1154.

Spear, R.C., Grieb, T.M., Shang, N., 1994. Parameter uncertainty and interaction in complex environmental models. Water Resour. Res. 30 (11), 3159–3169. http://dx.doi.org/10.1029/94WR01732.

Steiner, G., Weber, A., Magele, C., 2004. Managing uncertainties in electromagnetic design problems with robust optimization. Magn., IEEE Trans. 40, 1094–1099. http://dx.doi.org/10.1109/TMAG.2004.824556.

Tan, W., Chen, T., Marquez, H.J., 2002. Robust controller design and pid tuning for multivariable processes. Asian J. Control 4.

Wan Daud, W., Rosli, R., Majlan, E.H., Hamid, S., Mohamed, R., 2017. PEM fuel cell system control: A review. Renew. Energy 113, http://dx.doi.org/10.1016/j.renene.2017.06.027.

Wang, X., Curry, D., 2012. A robust approach to the share-of-choice product design problem. Omega 40, http://dx.doi.org/10.1016/j.omega.2012.01.004.

Yang, Z., Li, H., Li, Y., Li, Y., Chang, Y., Li, Q., Yang, K., wu, G., Sahoo, N., Poenisch, F., Gillin, M., Zhu, X., Zhang, X., 2019. Statistical evaluation of worst-case robust optimization intensity-modulated proton therapy plans using an exhaustive sampling approach. Radiation Oncology 14, http://dx.doi.org/10.1186/s13014-019-1335-8.

Zhang, J., Wu, J., Zhang, J., 2013. The Effects of Temperature on PEM Fuel Cell Kinetics and Performance. pp. 121–141. http://dx.doi.org/10.1016/B978-0-444-53688-4.00004-8.